

SERI/TR-253-3196
DE88001171

June 1988

KOLB

High-Temperature Solar Central Receivers for Electricity Production

J. V. Anderson
N. Weaver



SERI

Solar Energy Research Institute

A Division of Midwest Research Institute

1617 Cole Boulevard
Golden, Colorado 80401-3393

Operated for the
U.S. Department of Energy
under Contract No. DE-AC02-83CH10093

SERI/TR-253-3196
UC Category: 235
DE88001171

High-Temperature Solar Central Receivers for Electricity Production

J. V. Anderson
N. Weaver

June 1988

Prepared under Task No. ST712831

Solar Energy Research Institute

A Division of Midwest Research Institute

1617 Cole Boulevard
Golden, Colorado 80401-3393

Prepared for the
U.S. Department of Energy
Contract No. DE-AC02-83CH10093

NOTICE

This report was prepared as an account of work sponsored by the United States Government. Neither the United States nor the United States Department of Energy, nor any of their employees, nor any of their contractors, subcontractors, or their employees, makes any warranty, expressed or implied, or assumes any legal liability or responsibility for the accuracy, completeness or usefulness of any information, apparatus, product or process disclosed, or represents that its use would not infringe privately owned rights.

Printed in the United States of America
Available from:
National Technical Information Service
U.S. Department of Commerce
5285 Port Royal Road
Springfield, VA 22161

Price: Microfiche A01
Printed Copy A05

Codes are used for pricing all publications. The code is determined by the number of pages in the publication. Information pertaining to the pricing codes can be found in the current issue of the following publications, which are generally available in most libraries: *Energy Research Abstracts (ERA)*; *Government Reports Announcements and Index (GRA and I)*; *Scientific and Technical Abstract Reports (STAR)*; and publication, NTIS-PR-360 available from NTIS at the above address.

PREFACE

The research and development described in this document was conducted within the U.S. Department of Energy's Solar Thermal Technology Program. The goal of this program is to advance the engineering and scientific understanding of solar thermal technology and to establish the technology base from which private industry can develop solar thermal power production options for introduction into the competitive energy market.

Solar thermal technology concentrates the solar flux using tracking mirrors or lenses onto a receiver where the solar energy is absorbed as heat and converted into electricity or incorporated into products as process heat. The two primary solar thermal technologies, central receivers and distributed receivers, employ various point and line-focus optics to concentrate sunlight. Current central receiver systems use fields of heliostats (two-axis tracking mirrors) to focus the sun's radiant energy onto a single, tower-mounted receiver. Point focus concentrators up to 17 meters in diameter track the sun in two axes and use parabolic dish mirrors or Fresnel lenses to focus radiant energy onto a receiver. Troughs and bowls are line-focus tracking reflectors that concentrate sunlight onto receiver tubes along their focal lines. Concentrating collector modules can be used alone or in a multimodule system. The concentrated radiant energy absorbed by the solar thermal receiver is transported to the conversion process by a circulating working fluid. Receiver temperatures range from 100°C in low-temperature troughs to over 1500°C in dish and central receiver systems.

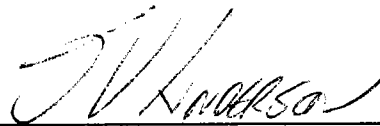
The Solar Thermal Technology Program is directing efforts to advance and improve each system concept through solar thermal materials, components, and subsystems research and development and by testing and evaluation. These efforts are carried out with the technical direction of DOE and its network of field laboratories that works with private industry. Together they have established a comprehensive, goal-directed program to improve performance and provide technically proven options for eventual incorporation into the Nation's energy supply.

To successfully contribute to an adequate energy supply at reasonable cost, solar thermal energy must be economically competitive with a variety of other energy sources. The Solar Thermal Program has developed components and system-level performance targets as quantitative program goals. These targets are used in planning research and development activities, measuring progress, assessing alternative technology options, and developing optimal components. These targets will be pursued vigorously to ensure a successful program.

This report documents the results of a study that examined the economic and technical potential of high-temperature solar central receiver systems for producing electricity. High-temperature central receivers were studied because significantly higher engine efficiencies result from operation at higher temperatures, and near-term advancements in engine technology promise to raise these efficiencies even more. Innovative solar thermal receiver and heat exchanger designs are required to achieve these high

temperatures. If these can be realized, the potential exists for dramatically advancing the competitiveness of solar thermal technology in electricity production. In addition to the potential for electricity production demonstrated in this report, these receiver technologies may also be valuable in other applications that require high concentrations or high temperatures, such as direct chemical conversion.

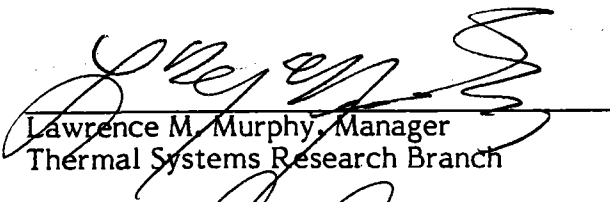
This report was prepared under the guidance of the DOE Division of Solar Thermal Technology. Review comments by Russ Skocypec and Craig Tyner of Sandia National Laboratories, Kevin Drost of Pacific Northwest Laboratories, Pascal DeLaquil III of Bechtel National, Inc., and Arlon Hunt of Lawrence Berkeley Laboratory were very helpful in clarifying the contents of the report. Also, the technical data provided by DFVLR, West Germany, within the IEA/AAPA project cooperation was helpful in assessing the volumetric receiver concept.



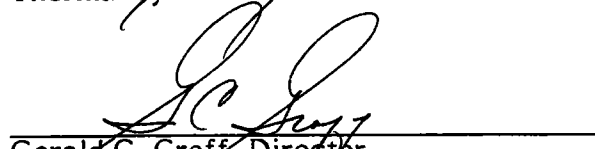
John V. Anderson

Approved for

SOLAR ENERGY RESEARCH INSTITUTE



Lawrence M. Murphy, Manager
Thermal Systems Research Branch



Gerald C. Groff, Director
Solar Heat Research Division

SUMMARY

Objective:

This report documents the results of a study on the technical and economic potential of high-temperature central receiver systems for electricity production.

Discussion:

Three advanced high-temperature (1000°-1400°C) central receiver concepts were included: the high-temperature direct absorption receiver (DAR), the particle injection receiver (PIR), and the volumetric receiver. Each of these receivers was coupled with an intercooled steam-injected gas turbine (ISTIG) engine mounted on a tower. Several permutations of the air heating systems (for the particle injection and volumetric receivers) were analyzed, including a case in which the ceramic air-to-air heat exchanger* (AAHX) was replaced with a liquid loop and two direct-contact heat exchangers (DCHX).

Currently, none of these high-temperature receivers has advanced beyond the conceptual level. Little, if any, empirical data about their performance and cost are available. As such, a number of simplifying assumptions have been made where data were not available or where more detailed calculations would not have significantly altered the conclusions. Consequently, the analysis summarized in this report is intended only to provide a preliminary assessment of the potential for these technologies. It is not intended to produce either a definitive design or a final prediction of capabilities.

The figure of merit used to compare the systems was the levelized energy cost, and the standards of comparison were a low-temperature (550°C) DAR and the U.S. Department of Energy's Solar Thermal Technology Program's long-term cost goal for electricity production (\$0.05/kWh).

All of the systems analyzed in this effort have a number of major technical uncertainties and research issues that would require resolution before major system development could be supported. The major uncertainty for the high-temperature DAR and the DCHX is that a high-temperature working fluid has not yet been identified. Similarly, there are several facets of the PIR design, including some of the particle cloud radiative characteristics and fluid dynamics, that need better definition. The uncertainties for the volumetric receiver included poor definition of the heat-transfer mechanisms in the fiber pack and uncertainty about the service characteristics of the fibers in this hostile environment.

The results indicated that subject to the caveats previously mentioned, the combination of advanced high-temperature receivers with an ISTIG engine does have the potential to be competitive with the low-temperature DAR and to meet the cost goal. In particular, the PIR with the DCHX produced a levelized energy cost that was almost 30% lower than the low-temperature DAR and was lower than the cost goal, although three other systems (the high-temperature DAR, the PIR with the AAHX, and the volumetric receiver with turbine exhaust inlet and DCHX) all produced about the same levelized energy cost as the low-temperature DAR.

*Used to transfer the energy from the atmospheric-pressure receiver stream into the high-pressure engine stream.

Although our analysis of the PIR with a DCHX resulted in a very good levelized energy cost prediction, the uncertainty in the cost and performance assumptions used in reaching these results must be recognized. For example, this system requires significant advancements in two different technologies: the particle/airstream interaction with the solar radiation and the high-temperature liquid-to-air DCHX.

The DCHX emerged from the results as a potentially important element of any high-temperature system. All of the best performing systems in this study used the DCHX. Compared with currently available ceramic heat exchangers (as represented by the AAHX), it provided both lower receiver outlet temperatures and lower cost. In addition, although not investigated here, the DCHX provides the potential for liquid storage with an air heating receiver.

Conclusions and Recommendations:

Based on this analysis, PIR appears to have potential cost and performance advantages over the high-temperature DAR and the volumetric receiver for high temperatures. The comparison between the PIR and the volumetric receiver is very direct since both produce hot atmospheric-pressure air. Further analysis of the volumetric receiver losses would have to show large improvements over the values calculated here before the volumetric receiver would begin to look attractive for electric power production. However a recent and more rigorous analysis of the volumetric receiver heat transfer conducted by Skocypec, Boehm, and Chavez showed that the losses ascribed to the volumetric receiver in this analysis may be too small. This would make the volumetric receiver system even less attractive.

The uncertainties associated with these systems are probably large enough to discourage near-term initiation of a major program effort in high-temperature central receivers for electricity generation. However, several low-level activities have been identified that should provide large payoffs leading to better understanding and use of solar thermal systems in general with minimal investment. They include:

- Analytic and laboratory-scale examination of the particle absorption and fluid mechanics issues raised by the PIR concept
- A preliminary survey of high-temperature liquids for the high-temperature DAR and DCHX
- Continuation of current investigations into the mechanics of direct-contact heat exchange
- Further investigation of the volumetric receiver performance using models like that developed by Skocypec, Boehm, and Chavez.
- The tracking of the development of high-efficiency engines (such as the ISTIG) outside the solar program.

Although the potential for reductions in the levelized energy cost for electricity may provide the primary motivation for pursuing at least a low level of high-temperature central receiver efforts, establishment of a body of data on these technologies may also provide an entry point for other applications. For example, many direct conversion and fuels and chemicals concepts will require elements that are similar to that considered in this analysis. Thus, the activities listed here could potentially provide even a larger payoff than is immediately apparent in the context of electricity generation.

TABLE OF CONTENTS

	<u>Page</u>
1.0 Introduction	1
2.0 System Descriptions	4
2.1 Low-Temperature DAR	4
2.2 Tower-Mounted ISTIG Engine	4
2.3 High-Temperature DAR	5
2.4 Particle Injection Receiver	6
2.5 Volumetric Receiver	10
3.0 Performance Analysis	14
3.1 High-Temperature DAR	15
3.2 Particle Injection Receiver	16
3.3 Volumetric Receiver	17
4.0 Cost Estimates	20
4.1 Costs from the Cost Goals	20
4.2 Receiver and Conversion Costs	21
5.0 Results	24
5.1 Performance Results	24
5.2 Levelized Energy Cost	26
6.0 Conclusions and Recommendations	30
6.1 Conclusions	30
6.2 Recommendations	30
6.3 Technical Uncertainties	31
7.0 References	32
Selected Distribution List	71

LIST OF FIGURES

	<u>Page</u>
1-1 Schematic of the base ISTIG engine	2
2-1 Shaft work efficiency of the ISTIG engine	5
2-2 Schematic of the high-temperature DAR system	6
2-3 Schematic of the PIR system	7
2-4 Streamlines and isotherms for a cross-section at the vertical centerline of the PIR	8
2-5 Heat fluxes, particle temperature, and particle radius along a single streamline just behind the PIR aperture	9
2-6 Schematic of the PIR/DCHX system	10
2-7 Temperature profiles of the fibers and the air through the volumetric receiver fiber pack for ambient temperature inlet air	11
2-8 Schematic of the VR/amb system	12
2-9 Schematic of the VR/tb-ex system	13
2-10 Schematic of the volumetric receiver/DCHX system	13
3-1 Flowchart of the high-temperature DAR design process	15
3-2 Levelized energy cost as a function of aperture area for the high- temperature DAR system	16
3-3 Infrared emission loss curves for the volumetric receiver	17
3-4 Comparison of loss curves from Karrais and Skocypec, Boehm, and Chavez	19
4-1 Breakdown of the system capital costs by subsystem	23
5-1 Annual thermal-to-electricity efficiency from insolation incident on the heliostats to net electricity	25
5-2 Cumulative subsystem efficiency bar charts (waterfall charts) for all of the systems	25
5-3 Levelized energy costs: (a) values in $\$/kW_e$ and (b) values normalized to that of the low-temperature DAR system	27
5-4 Sensitivity of the levelized energy cost results to increased heliostat costs	28

LIST OF FIGURES (Concluded)

	<u>Page</u>
5-5 Sensitivity of the levelized energy cost results to the cost of the high-temperature DAR	28
5-6 Sensitivity of the levelized energy cost results to the cost of the DCHX	29

LIST OF TABLES

	<u>Page</u>
4-1 Development of System Capital Costs.....	20
4-2 Levelized Energy Cost Economic Scenario Assumptions.....	21
4-3 Source of Cost Estimates for the Receiver and Conversion Cost Categories	22
B-1 Major Technical Uncertainties	67

1.0 INTRODUCTION

Several recent studies have examined the potential for using solar central receivers to generate high-temperature energy. Generally they have been unable to identify any significant advantage to producing high temperature energy for either electricity production or industrial process heat [1-5].

For industrial process heat, the increased receiver losses (and decreased efficiency) at higher temperatures cause the cost of solar-generated energy to increase above that of the competitive fossil sources. The problem is particularly acute since the cost of the fossil-generated energy does not generally increase with temperature [6]. Similarly, the principal problem for high-temperature solar electricity generation has been that the increase in conversion cycle efficiency possible at higher inlet temperatures (e.g., 900°-1300°C) is more than offset by the concomitant decrease in the solar energy system efficiency.

However, several recent advancements in technology, notably the development of very high efficiency engines and some new receiver concepts, provide the incentive to reexamine the potential of generating electric energy at high temperatures. The effort described here is an assessment of several of the more promising receiver concepts in combination with an advanced high-efficiency high-temperature engine design. In one sense it is an update to previous work and will provide a clearer picture of the merits of proceeding with research on high-temperature central receiver concepts.

The intercooled steam-injected gas turbine (ISTIG) engine [7] is an interesting, recently proposed high-temperature engine. A schematic of the basic gas-fired engine is shown in Figure 1-1. The ISTIG engine incorporates several of the advantages of combined cycles (e.g., a Brayton-Rankine system) but avoiding much of the expense associated with purchasing two complete engines.

In the simplest description of the ISTIG concept, the enthalpy remaining in the power turbine exhaust stream (about 440°C and atmospheric pressure at design conditions) is used to generate steam at about 500 psi. This steam is then mixed with the high-pressure airstream from the compressor discharge, heated, and expanded through the high-pressure and power turbines* increasing the shaft output. In this way, efficiencies equal to those available from combined cycles (on the order of 55%) can be achieved, potentially at much lower capital costs.

A version of this engine that is not intercooled is currently available from General Electric [8] with a thermal-to-electricity conversion efficiency of at least 43% guaranteed by the manufacturer. Conversations with General Electric engineers [9] have established that this version has been quite successful. They also indicated that some analysis work on the intercooled version had already taken place, and a serious development program leading to an engine with a guaranteed efficiency of at least 52% (thermal energy to electricity, based on the lower heating value) was likely to begin in 1988 and would require roughly four years. Thus, the engine efficiencies used for this effort represent relatively near-term values that should be achievable with off-the-shelf hardware within a few years.

*This is, of course, a very simplistic description of the steam flowpath. In fact, the steam is introduced into the airstream in a number of locations that extend from before the combustor region well into the power turbine region.

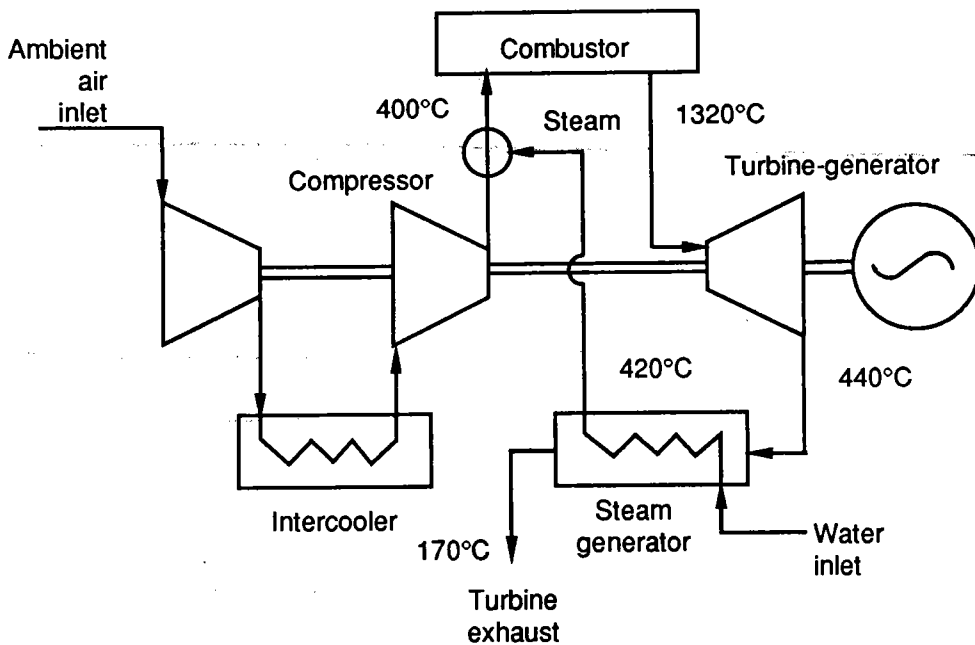


Figure 1-1. Schematic of the base ISTIG engine

Three receiver concepts are examined in this work. They each promise greater efficiency at high temperatures than high-temperature receivers studied previously. In addition, they promise to be more robust to the adverse effects of high fluxes, high temperatures, and transient conditions than the current generation of tubular receivers. Although these improvements are achieved by several techniques, they generally involve absorbing the radiation more directly into the working fluid, effectively removing the intermediate transfer through the tube wall. In this way, the receiver thermal losses are reduced and the response of the system to transients is improved.

The intent of this study was to examine the long-term potential of several high-temperature systems for delivering electric power. It is important to recognize that this current effort is a preliminary assessment. As such, no effort was made to try every possible promising system configuration nor was a great deal of effort expended on optimizing the details of the configurations presented here. In fact, each of the systems examined here has a number of technical uncertainties that necessitated making important assumptions about the cost and performance. These uncertainties are examined in Section 6.3 and Appendix B.

One of the major ground rules of this study bears special mention. None of the high-temperature systems examined here used any storage. Although this might appear like a gap in the work, this assumption was made for several reasons. First of all, the addition of thermal storage would have required adding several elements to the analysis that, because of the difficulty in quantifying them, would have added substantially to the uncertainty of the results. For example, the cost, efficiency, and parasitic losses associated with high-temperature transport and storage systems would have to have been estimated. Also, because the relative cost of transport and storage would likely be much higher than for conventional 550°C systems, the optimum solar multiple and storage size would need to be individually determined for each system.

Second, the addition of storage is unlikely to affect the conclusions of the study. For example, the most promising systems all involved the direct-contact heat exchanger (DCHX), which opens the possibility of using liquid storage. Since this option would be equally available to all of these systems it would not change the comparisons between them. Similarly, both of the air-heating systems (particle injection and volumetric receivers) with the air-to-air heat exchanger (AAHX) could use the same storage medium (e.g., ceramic bricks), so adding storage would not help distinguish between them.

The one area that the addition of storage might have affected is the comparison between the high-temperature systems and the low-temperature direct absorption receiver (DAR). However, since the conclusions of the study are already fairly positive about the potential of the high-temperature systems, the only effect would be to strengthen the conclusions. Overall then, although the possibility of storage (either directly from hot air into ceramic bricks or in liquid from a DCHX or high-temperature DAR system) was recognized, these options were not pursued.

2.0 SYSTEM DESCRIPTIONS

This section describes the technical details of the systems analyzed in this work. The primary basis for comparison was the low-temperature DAR [10], which is described very briefly here. Three high-temperature receiver concepts were examined: the high-temperature DAR [10,11], PIR [12] (also see Appendix A), and the volumetric receiver [13,14].

All of the high-temperature systems examined here use a tower-mounted ISTIG engine directly coupled to the solar receiver by a heat exchanger. Thus, the three receiver concepts are examined in their simplest configuration: strict sun-following with no storage. The following sections examine the characteristics of the ISTIG engine, describe each of the receiver concepts, and detail how the receivers were mated with the ISTIG engine.

2.1 Low-Temperature DAR

The major basis of comparison for the high-temperature systems examined here was a low-temperature (550°C) DAR system similar to the one considered in Anderson et al. [10]. The direct absorption concept involves absorbing the concentrated insolation directly into a film of darkened, molten nitrate salt flowing over a nearly vertical plate. Other than the low-temperature DAR, this system was of largely conventional design for nitrate salt systems. The heated salt is collected in a hot-salt storage tank, which feeds a steam generator for the Rankine engine. The cold salt is then collected in another tank before being pumped back to the tower top.

The peak and average flux levels on the low-temperature DAR were 1.8 MW/m^2 and 0.8 MW/m^2 , respectively. The low-temperature DAR was sized to have a rated power level ($196 \text{ MW}_{\text{th}}$) that is the same as the high-temperature receivers. With a solar multiple of 1.8, the resulting EPGS rated size is 45.5 MW_e . The storage was sized for 7 h of rated operation.

2.2 Tower-Mounted ISTIG Engine

The rated output of the ISTIG engine under design conditions is 110 MW_e (more than twice that of the low-temperature DAR system). The turn-down ratio of the ISTIG engine was estimated to be 4:1. This is probably conservative since the ISTIG design is developed from an aircraft (DC-10) engine where substantially larger turn-down ratios are required. At design power the state conditions of the air-steam mixture at the inlet to the high-pressure turbine (the hottest point in the system) are 1350°C and more than 30 atm.

Although the 56% design point efficiency of the ISTIG engine is a very attractive feature, the off-design or part load performance may be more important for solar applications. Figure 2-1 shows the thermal-to-shaft work efficiency* as a function of the turn-down ratio. The points indicated were drawn from the Pacific Gas and Electric Company (PG&E) report [7], and the line represents the curve fit used to extrapolate the data down to lower turn-down ratios. The engine efficiency remains quite high over the entire turn-down range, decreasing to only 47% at the full turn-down ratio.

*The final thermal-to-electricity efficiency also included a generator efficiency of 98%.

Because the intercooled steam-injected engine is gas turbine, it requires very little time or energy to start. Informal estimates from General Electric engineers indicated that the engine could be running as a simple cycle gas turbine (with lower efficiency—36%) in something less than 5 min and could be warmed up and operating in the steam-injection mode in another 15 min. Although the solar heat exchangers would require some time to warm up before the engine could be started, this might be accomplished under insolation levels too low to operate the engine. Somewhat conservatively, a simple start-up time of 30 min (from the advent of insolation levels large enough to start the engine) was used for each of the systems, and no credit was taken for the derated-lower efficiency operation during the time required to heat up the steam generator.

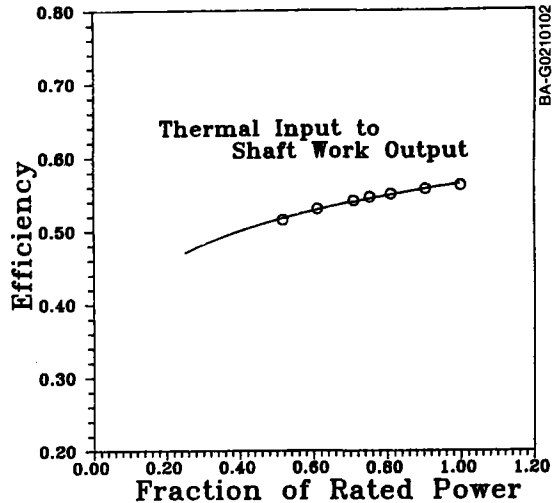


Figure 2-1. Shaft work efficiency of the ISTIG engine. The data points indicated are from General Electric. The curve indicates the part-load efficiency assumed here.

Similarly, although response to transients would be slowed somewhat by the intercooler and the steam generator, the ISTIG engine should be able to follow transients quite quickly. The performance simulations for this work were run at 0.25-h time steps, and it was assumed that the engine could follow any transients present on that time scale.

The major assumption made in modeling the ISTIG engine is that an externally fired version of this engine can be developed that would have the same efficiencies as projected for the in-line fired version. Although externally fired gas turbines are reasonably common, there currently does not appear to be any externally fired version of this engine either with or without the steam injection. The overall attitude of the General Electric engineers was that developing an externally fired version would probably be simpler than developing the intercooled version, since fewer changes to the compressor and turbine wheels would be required.

2.3 High-Temperature DAR

The high-temperature DAR is very similar to the low-temperature DAR. However, once the energy is collected in the working fluid, it is then transferred into the high-pressure air from the compressor in a DCHX, as shown in Figure 2-2. After passing through the turbine, the exhaust is used to raise steam, which is injected back into the engine just as in the original fossil-fired ISTIG engine configuration.

In addition to its low cost, one of the major advantages of the DCHX for the high-temperature DAR is that it transfers heat quite effectively. For this reason the outlet temperature of the cold stream (to the turbine) is essentially the same as the inlet temperature of the hot stream (from the receiver) [15]. Since the performance of the high-temperature DAR is fairly sensitive to the receiver outlet temperature, keeping it as low as possible is an important feature.

Identification of a working fluid for this high-temperature DAR application is a major uncertainty associated with this system (as well as with all of the DCHX systems

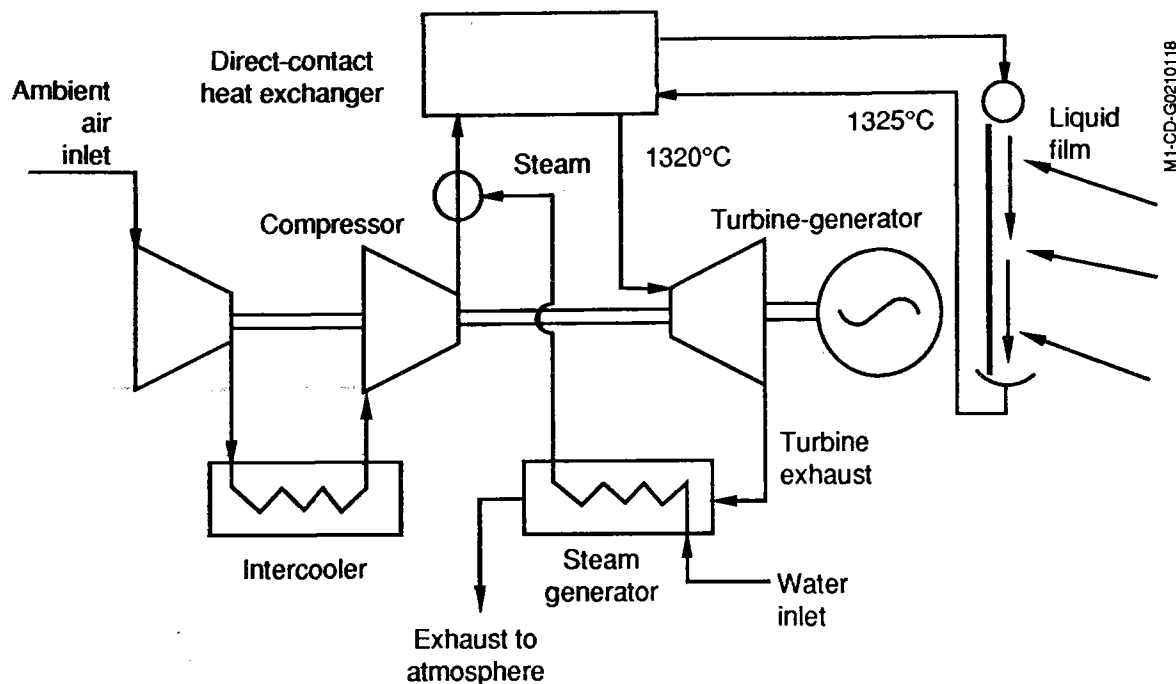


Figure 2-2. Schematic of the high-temperature DAR system

examined here). The qualities required from candidate fluids are challenging: in addition to simply operating over a very large temperature range, the fluid must be stable in intimate contact with hot air-steam mixtures, it must be compatible with materials needed for containment and pumping systems, and it must not form droplets or foam (since carryover of the fluid from the heat exchanger into the turbine could be a very serious problem).

Although little work has been done on identifying working fluids for this application, one preliminary candidate, a molten glass, B_2O_3 , has been proposed. Based on data from Maru et al. [16], this compound has a higher heat capacity and a lower cost per pound than the nitrate salt mixture frequently considered for conventional receivers. The same source lists the melting temperature of B_2O_3 as 450°C . Although this melting temperature is somewhat high for this application (the temperature of the mixed air-steam into the DCHX is about 400°C), it likely could be improved by mixing with other glass compounds in a eutectic mixture much as salts are mixed. However, a thorough search for other suitable fluids needs to be conducted before any judgments can be made.

2.4 Particle Injection Receiver

The particle injection receiver (PIR) configuration used here was developed for the Solar Energy Research Institute (SERI) by Bechtel National, Inc., and is based on conceptual work performed by Hunt at Lawrence Berkeley Laboratories [17]. A copy of Bechtel's report is Appendix A and contains more details about the design process, the receiver loss analysis, and the cost estimates.

A schematic of the PIR concept is shown in Figure 2-3. In this system the turbine exhaust stream is used as the receiver inlet. A small amount (less than 0.5% by weight) of very small ($0.3 \mu\text{m}$) carbon particles is injected into the receiver inlet stream to make it optically dark. This stream is then drawn upward past the aperture of the receiver,

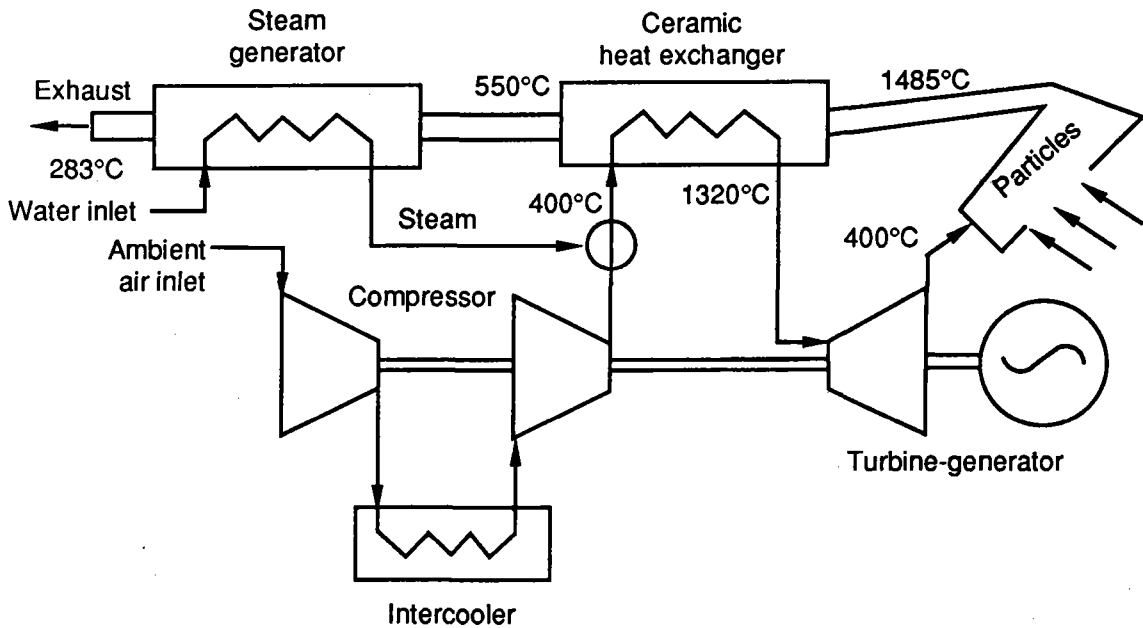


Figure 2-3. Schematic of the PIR system

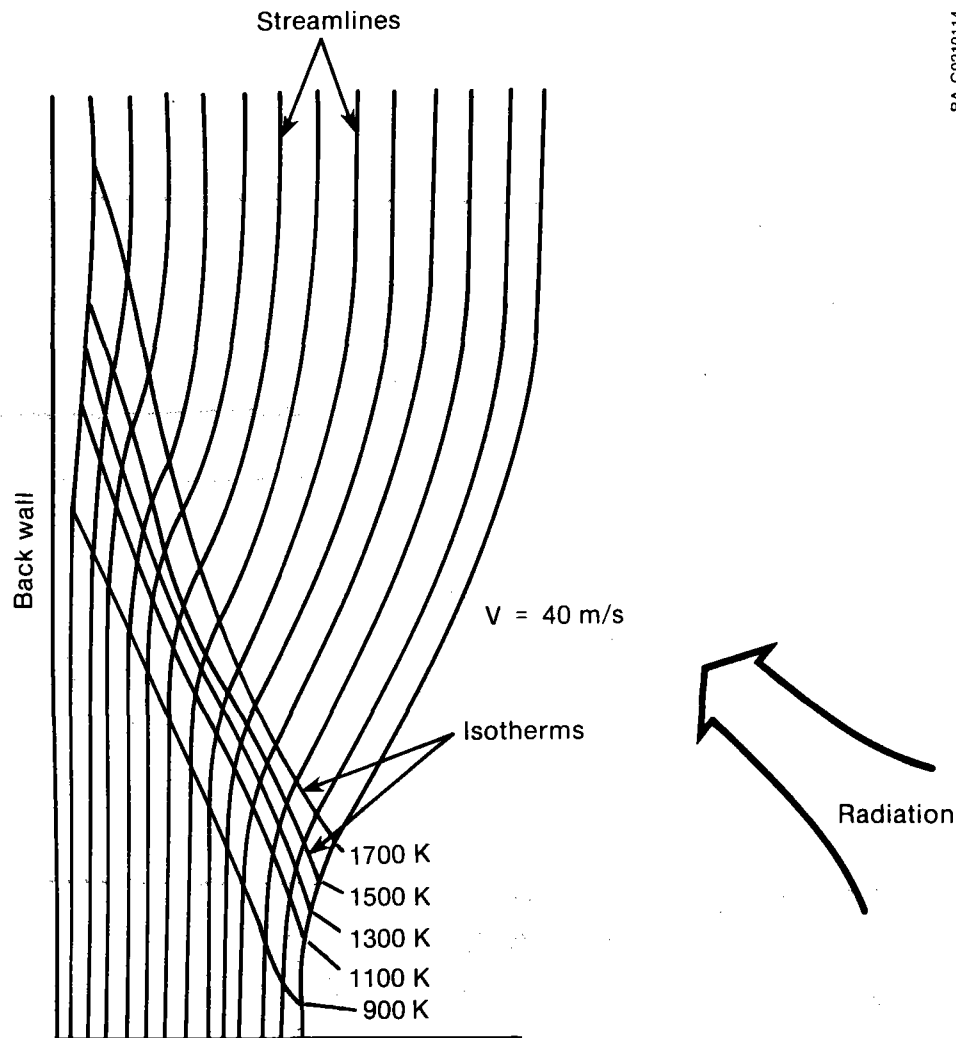
where the radiation is absorbed by the small particles, which transfer the energy convectively into the air before oxidizing to form water and carbon dioxide. Because the particles are so small, the convective coupling with the air is quite efficient, and the air and particle temperatures are essentially equal.

The front surface of the particle cloud is protected from mixing with the ambient air by an air curtain, a layer of air without particles that travels along in front of the particle cloud at the same velocity. This layer of the flow is collected separately from the heated air at the top of the aperture.

Figure 2-4 shows the streamlines and isotherms predicted for a vertical cross-section of the flow path. Because the particle cloud is optically dense, the incident radiation does not penetrate more than about one-tenth of the front-to-back dimension of the receiver. Thus the particles along the front streamline (right-most in the figure) are heated the most rapidly. At some temperature (depending on design conditions), these front particles oxidize and disappear, exposing the next layer of particles. Thus, the front surface of the particle cloud moves toward the back wall as the gas flows upward, and has a cross-sectional contour much like the highest isotherm in Figure 2-4.

Above the point where the particles oxidize and disappear, the remaining gases are largely transparent* to the radiation, and the temperature remains nearly constant. The particle injection can be controlled so the last particles will be just disappearing as the flow leaves the top of the aperture. However, oxidation of the particles by the hot air will continue even without the solar radiation, so any particles remaining in the stream will likely be consumed shortly after leaving the aperture.

*Dry air is very transparent to almost all wavelengths of radiation. However, water vapor does have some appreciable absorptance. The analysis by Bechtel for this design did not include the effect of the steam in the turbine exhaust. However, hand calculations by Bechtel demonstrated that the addition of the steam to the analysis will produce effects that offset each other. This is documented in Section 5.1 of Appendix A.



BA-G0210114

Figure 2-4. Streamlines and isotherms for a cross-section at the vertical centerline of the PIR. After the small carbon particles are oxidized, the air is no longer heated, hence, the shape of the isotherms. Developed by Bechtel National, Inc. (see Appendix A).

The radiative characteristics of these very small particles are substantially different than the characteristics of either larger particles or solid surfaces made from the same material (e.g., solid carbon). Because the particle diameter is on the same order as, or smaller than, the wavelength of the light incident on them, their behavior is predicted by the Mie theory, which is well described in the literature (e.g., see Bohren and Huffman [18]). One of the important features of this regime is that the absorption and emission of radiation by these small particles vary as the inverse of the wavelength. Thus, the absorption of the short wavelength solar radiation is quite high, while the emission of the longer wavelength infrared radiation is substantially smaller. This selective absorption mechanism imparts a significant advantage to the PIR concept, particularly for high-temperature operation where the infrared emission losses are most important.

The largest loss mechanism from this type of absorber is the back scattering of the radiation by the particles. In fact, scattering losses from the particles in this design are

about 13%-15%, which is larger than the reflection from some forms of solid carbon (e.g., carbon black). This is again a property of the small particles and is a fairly minor tradeoff for the low emissive losses in high-temperature systems.

These effects are demonstrated in Figure 2-5 where the radiation exchanges of the particles are plotted as a function of distance in the flow direction for a streamline at the front of the aperture. The solar radiation incident on this front streamline is shown at the top of the plot. Just below that is the absorbed radiation, which follows the incident radiation closely until the particle radius becomes quite small (see the radius and temperature plotted at the bottom). The next curve on the figure is the scattered radiation, which is roughly an order of magnitude smaller than the absorption. The emitted radiation has the lowest value and varies from one to several orders of magnitude smaller than the absorbed flux.

After being collected at the top of the aperture, the hot gas stream is fed through one side of a ceramic AAHX where it heats the compressor discharge stream. Because the effectiveness of this heat exchanger is less than 1.0 (0.85 in this case), the temperature of the stream leaving the receiver must be significantly (as much as 160°C) higher than the temperature of the stream going to the turbine. This increase in temperature is a disadvantage for both the PIR and the volumetric receiver when compared with the DCHX used in the high-temperature DAR concept.

After leaving the AAHX, the still-hot receiver gas stream (at about 550°C) enters the steam generator where it is used to generate the steam injected into the engine flow. Because the gas leaving the AAHX is hotter than the turbine exhaust temperature, more steam could be generated by this arrangement than is generated by the turbine exhaust in the original ISTIG concept. Unfortunately,

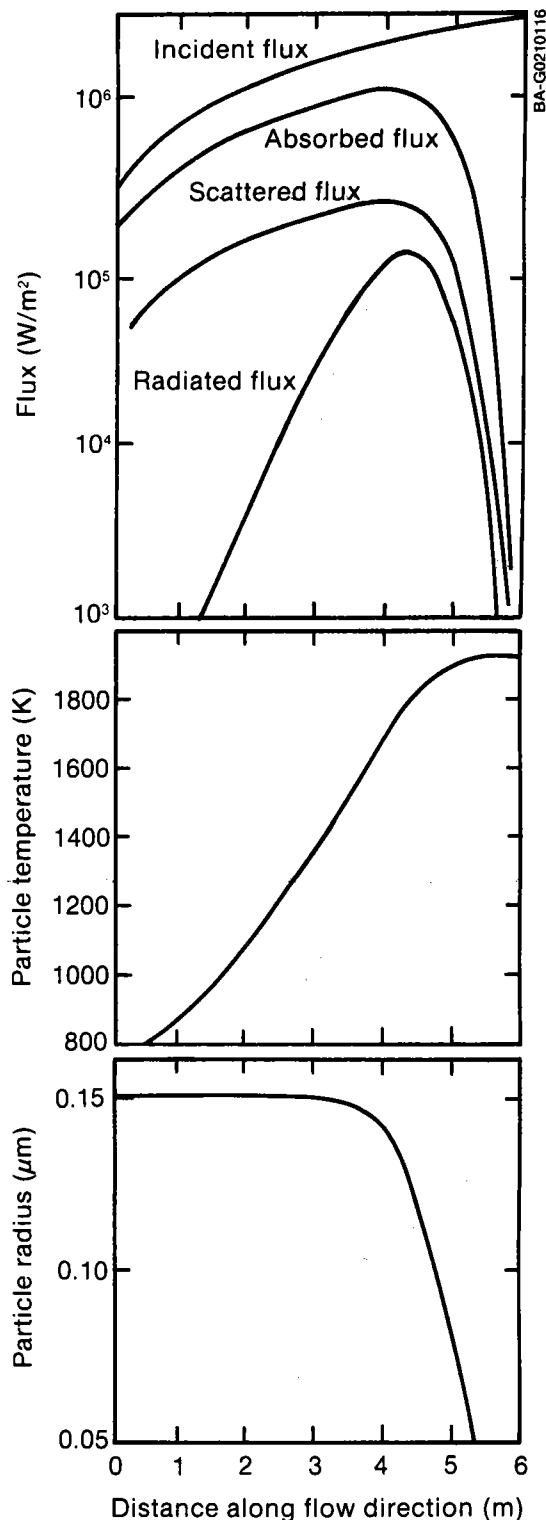


Figure 2-5. Heat fluxes, particle temperature, and particle radius along a single streamline just behind the PIR aperture. Note the disparity between the absorbed radiation and the emitted radiation. Developed by Bechtel National, Inc. (see Appendix A).

adjusting the available ISTIG performance information to account for the increased output from this extra steam was well beyond the scope of this study. As a consequence, the extra energy was lost in the form of a higher temperature exhaust stream from the steam generator.

However, a second PIR configuration that was identified by SERI during this study could eliminate this energy loss. In this configuration (PIR/DCHX), shown in Figure 2-6, the AAHX is replaced with two DCHXs, one operating at low pressure in the receiver stream and the other operating at high pressure in the engine stream. This configuration takes advantage of the close approach temperatures possible with direct-contact heat exchange to lower the receiver temperature and reduce losses caused by unnecessarily high exhaust temperature. It also requires a high-temperature liquid working fluid and the introduction of another fluid loop with a pump, probably a head-recovery expander, and the associated tanks and piping. (Note, however, that all of this equipment has already been assumed to be available for the high-temperature DAR.)

Because the turbine exhaust stream is used as the receiver inlet stream, the operation of the receiver and engine are more closely coupled for this system than for the high-temperature DAR. Although this coupling is technically and aesthetically appealing, it could conceivably cause control problems as the system tries to respond to rapidly changing external conditions. If this were perceived as a problem, the PIR could also be configured with various bypasses and alternate inlet streams as needed.

2.5 Volumetric Receiver

In the volumetric receiver, the radiation is absorbed in a series of grids composed of small diameter fibers. The density of the grids is adjusted so the concentrated radiation is absorbed throughout the depth of the fiber pack. As air is drawn through the fiber pack, it is heated convectively by the fibers.

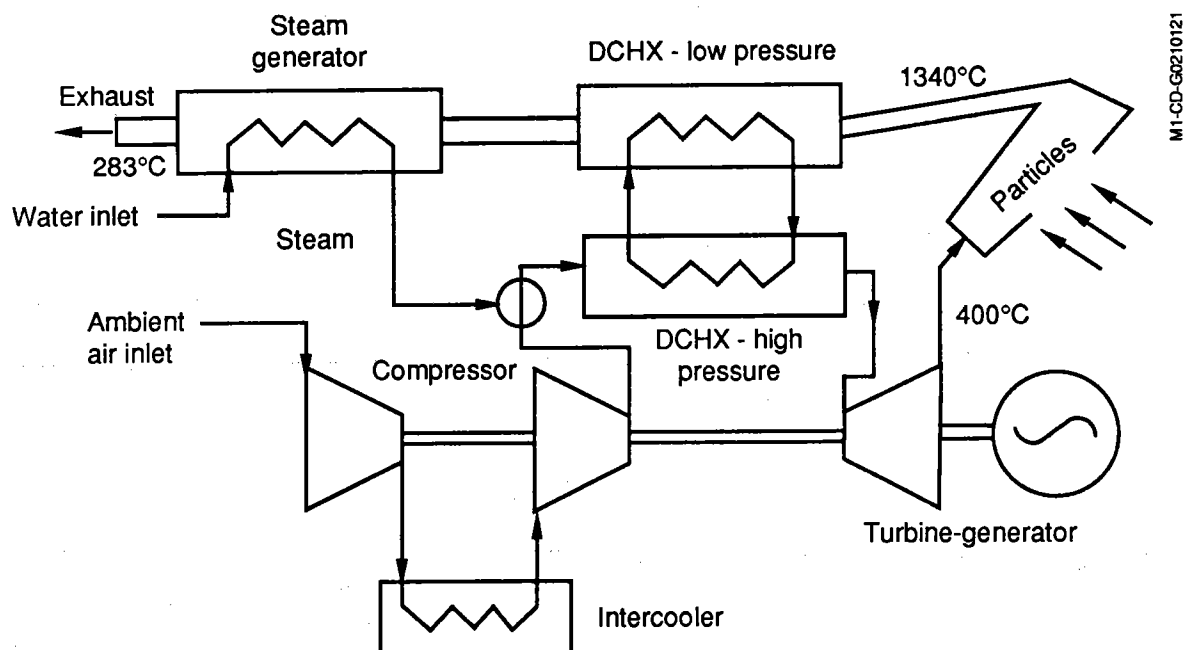


Figure 2-6. Schematic of the PIR/DCHX system. Note the two DCHXs replacing the air-to-air heat exchanger.

One important trade-off in the volumetric receiver involves the diameter of the fibers. As the diameter decreases, the convective transfer to the air becomes more efficient, but the mechanical strength of the fibers decreases. Since the fibers must be strong enough to withstand the air flow past them, and thick enough not to burn out under the concentrated radiation, their diameter becomes a crucial issue. The analysis here was based on the losses reported in Karrais [19] and assumed silicon carbide fibers with a diameter of 0.1 mm.

Figure 2-7 shows an example of the temperatures of the fibers and air for one of the cases studied by Drost [13]. Since the air comes in at near-ambient temperature and the fibers are coupled to the air by convection, the temperature of the front fibers is fairly low. Then, as the air moves toward the back of the fiber pack, it is heated and its temperature increases. The temperature of the fibers is held above the air temperature by the incoming solar radiation until it gets to the very back of the fiber pack. In this way the highest temperature fibers are "hidden" in the back of the fiber pack where they have the smallest view factor of the ambient. This has the effect of lowering the emissive losses.

As in the PIR, the energy in the atmospheric pressure air from the receiver is transferred to the high pressure air from the engine in a ceramic AAHX. Meanwhile, the turbine exhaust is used to raise the steam to be injected into the engine. Figure 2-8 is a schematic of a volumetric receiver system heating from the ambient (VR/amb). Notice that once the hot receiver air has been used to heat the engine air, it must be discharged to the ambient despite the fact that it is still rather hot (perhaps 400°-550°C). This fact, especially when combined with the low (0.85) effectiveness of the AAHX, causes the VR/amb to be significantly less efficient than the other systems. Because of this problem, it was clear that the performance of the VR/amb could not be competitive with the other systems, and this configuration was not included in the remainder of the analysis. However, there are at least two solutions to the VR/amb problems:

- The first is to use the hot exhaust to generate additional steam that could be expanded through the turbine. Unfortunately, because of the problems associated with adjusting the engine performance (as previously described), this could not be analyzed.

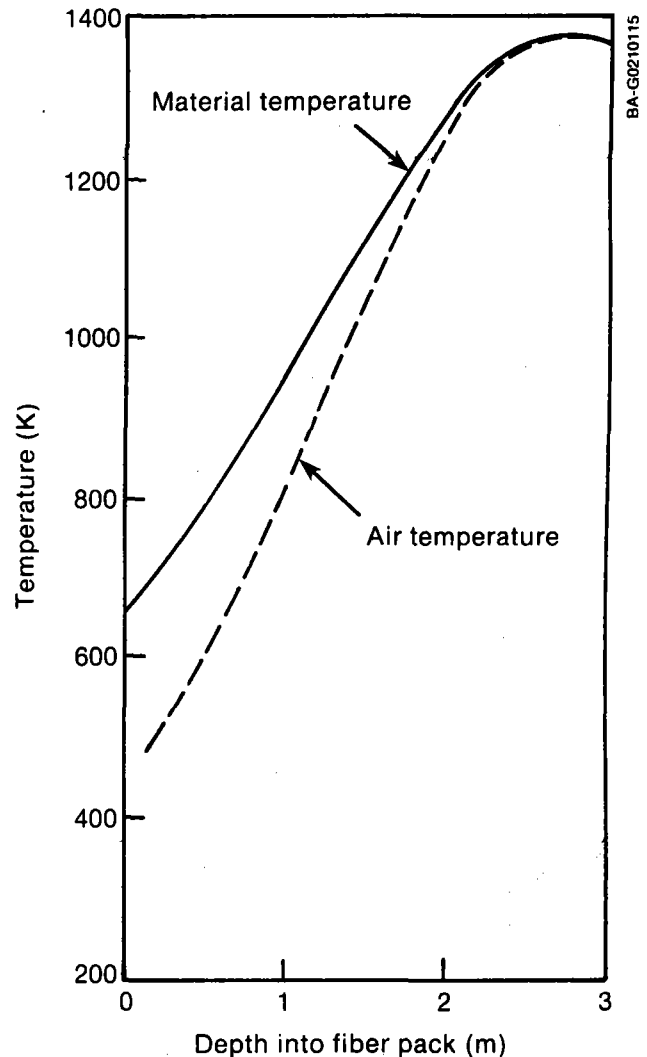


Figure 2-7. Temperature profiles of the fibers and the air through the volumetric receiver fiber pack for ambient temperature inlet air. Developed by Drost [13].

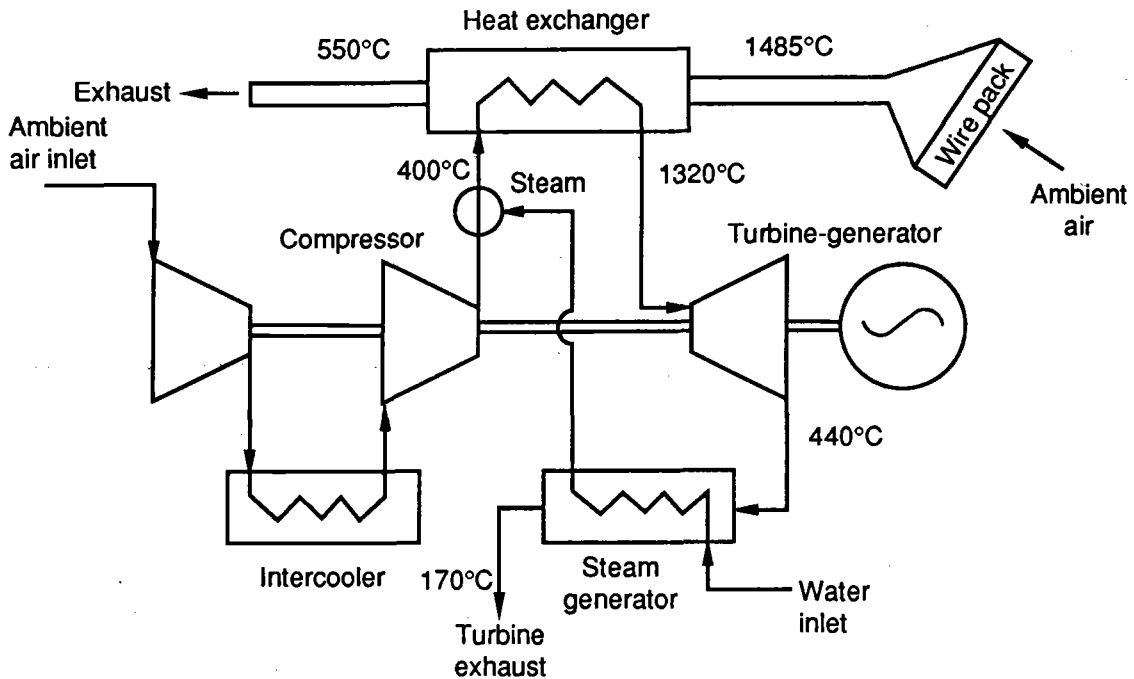
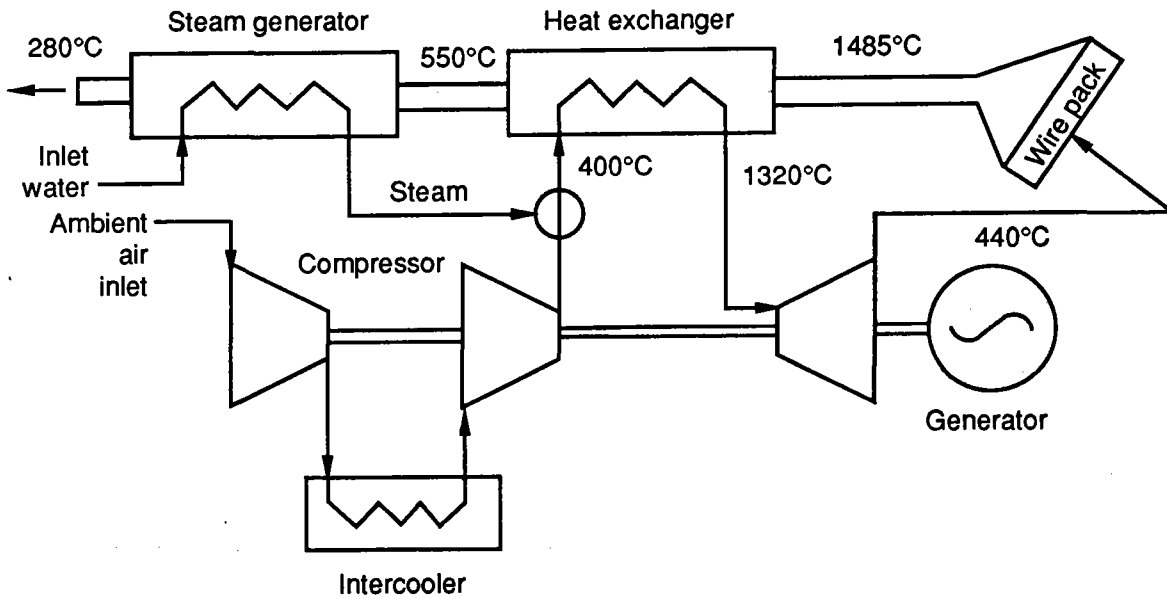


Figure 2-8. Schematic of the VR/amb system. Note the two separate exhaust streams (upper left and bottom center).

- Another possible permutation of the volumetric receiver system is to use the turbine exhaust as the receiver inlet, as was done with the PIR. This would allow both the field and the receiver to be smaller and would still allow more steam generation than the original ISTIG concept. However, a major feature of the volumetric receiver performance is the fact that the higher temperatures are partially "hidden" in the back of the fiber pack. This happens because the ambient temperature air keeps the front fibers cool. If the turbine exhaust (at about 450°C) were used as the inlet to the fibers, the temperature of the front fibers would go up and the losses would increase.

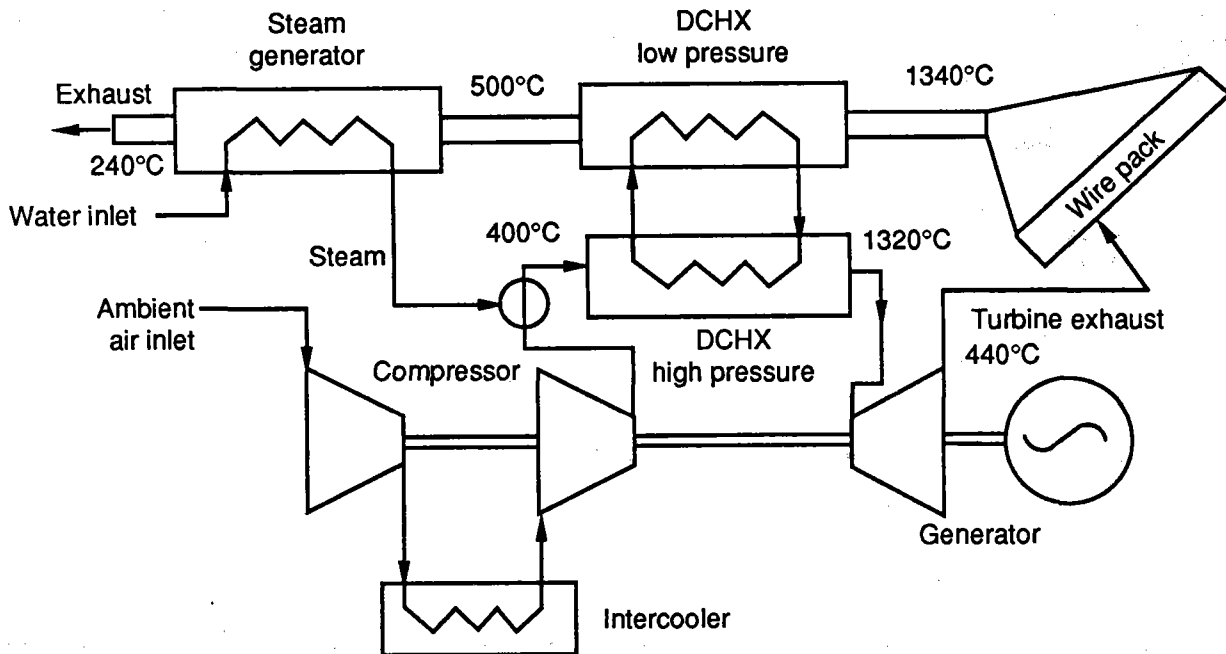
A schematic of this second possibility is shown in Figure 2-9. In this case, the turbine exhaust is used as the inlet stream to the volumetric receiver (VR/tb-ex) and the outlet of the AAHX is fed into the steam generator. Although this configuration avoids the obvious losses associated with the VR/amb, the lack of available analysis tools for the volumetric receiver precluded accurately accounting for the increased temperature of the front fibers with this preheated air (see Section 3.3). Therefore, the losses for this configuration were analyzed as though the incoming air were at ambient temperature, which produced somewhat optimistic loss estimates.

The second volumetric receiver configuration involves replacing the AAHX with two DCHXs, much as was done for the PIR/DCHX. This configuration is shown in Figure 2-10. Again, this configuration requires a high-temperature liquid working fluid and all the associated trappings. However, note that the decrease in receiver temperature has a larger effect on the volumetric receiver losses than on the PIR losses because the volumetric receiver loses substantially more energy by emission than the PIR.



M1-CD-G0210122

Figure 2-9. Schematic of the VR/tb-ex system. Note the exhaust from the turbine used as the inlet for the receiver.



M1-CD-G0210123

Figure 2-10. Schematic of the volumetric receiver/DCHX system

3.0 PERFORMANCE ANALYSIS

The performance analysis for this study entailed two principal tasks: (1) system sizing using the central receiver design code DELSOL [20] and (2) prediction of annual energy production using a version of the code SOLERGY [21] modified specifically for this study.

In general, the performance analysis of the high-temperature receiver/ISTIG engine systems required several departures from conventional central receiver design procedures. In the conventional design process, an initial design pass is made to select an approximate range of values for tower height, heliostat field size, and receiver aperture size given the design power rating for the plant. Then another search is made to select the receiver and field size so the system will deliver design point power and minimize the levelized energy cost. During this second stage, the aperture size is selected based on a trade-off between optical spillage losses, which decrease as the aperture is enlarged, and thermal losses, which increase as the aperture is enlarged. Since a Rankine-based central station solar power plant operates at a nominally fixed receiver outlet temperature, the conventional design cycle sizes the system for fixed design point conditions.

For the high-temperature systems examined here, the principal difficulty lies with the fact that the ISTIG engine operates over a range of temperatures as the input changes. For example, as the input power to the turbine varies from 25% to 100%, the turbine operating temperature varies from about 1030°C to 1350°C. This in turn causes both the receiver operating temperature and the receiver thermal losses to vary, so the receiver is frequently operating at off-design temperatures.

The first step in the performance analysis, system sizing, was carried out in a slightly different manner for each of the three receiver designs. The low-temperature DAR, high-temperature DAR, and volumetric receiver systems were configured by SERI staff members, and the PIR configurations were developed under subcontract by Bechtel National, Inc. However, for all of the systems, the central receiver design code DELSOL was used to develop field layouts given heliostat parameters, tower height, and other system descriptors.

The same heliostats were used in the analysis of all systems. The heliostats modeled were second generation glass and metal heliostats (58.5 m²) with a total reflected beam error of 4.6 mrad*.

The second step, annual energy prediction, was performed by SERI staff members. Once a system design was defined for each aperture size, the results were passed to a modified version of the SOLERGY code, SLGHIT, to estimate annual energy performance. In developing SLGHIT, the first modification to SOLERGY involved calculating the system operating point by balancing the incident flux, the receiver thermal losses, and the engine operating curves at each time step. Additionally, the SOLERGY dispatch strategy was rewritten to analyze a simple sun-following strategy with no storage.

The SLGHIT simulation was run on 15 min, 1985 weather data from Barstow, Calif. The operation of the heliostat field was captured in the form of a field efficiency table (azimuth and elevation angle vs. optical efficiency). Receiver thermal losses were characterized as a function of the operating temperature and were then input to SLGHIT.

*These heliostat characteristics were chosen to provide compatibility with the APS Saguaro repowering study [22].

Parasitic losses were evaluated on a component-by-component basis for each system. Common to each system was an estimate of field heliostat drive and control power requirements. Also common to each system were estimates for the power requirements of the ISTIG engine's intercooler pump and fan, fuel and water pumps, and balance of plant.

3.1 High-Temperature DAR

A tower height of 205 m was selected by DELSOL for the high-temperature DAR system based on initial estimates of receiver performance characteristics. The high-temperature DAR cavity was configured with a depth of about 4 m, which provided an average flux of about 0.83 MW/m^2 and a peak flux of 1.8 MW/m^2 . Field layout and aperture size are closely coupled to receiver loss estimates. As indicated in Figure 3-1, the selection of field and aperture size was accomplished by an iterative process. For the high-temperature DAR, radiation losses were calculated using the code RADSOLVER [23], and convection losses were estimated using the Kraabel correlation [22]. An initial estimate of thermal losses was used first as the basis for determining an initial field size. Then an incident flux map was produced for this field and was used to calculate improved thermal loss estimates. With these improved thermal loss estimates, a new field layout was generated along with a new flux map and new loss estimates until convergence was achieved.

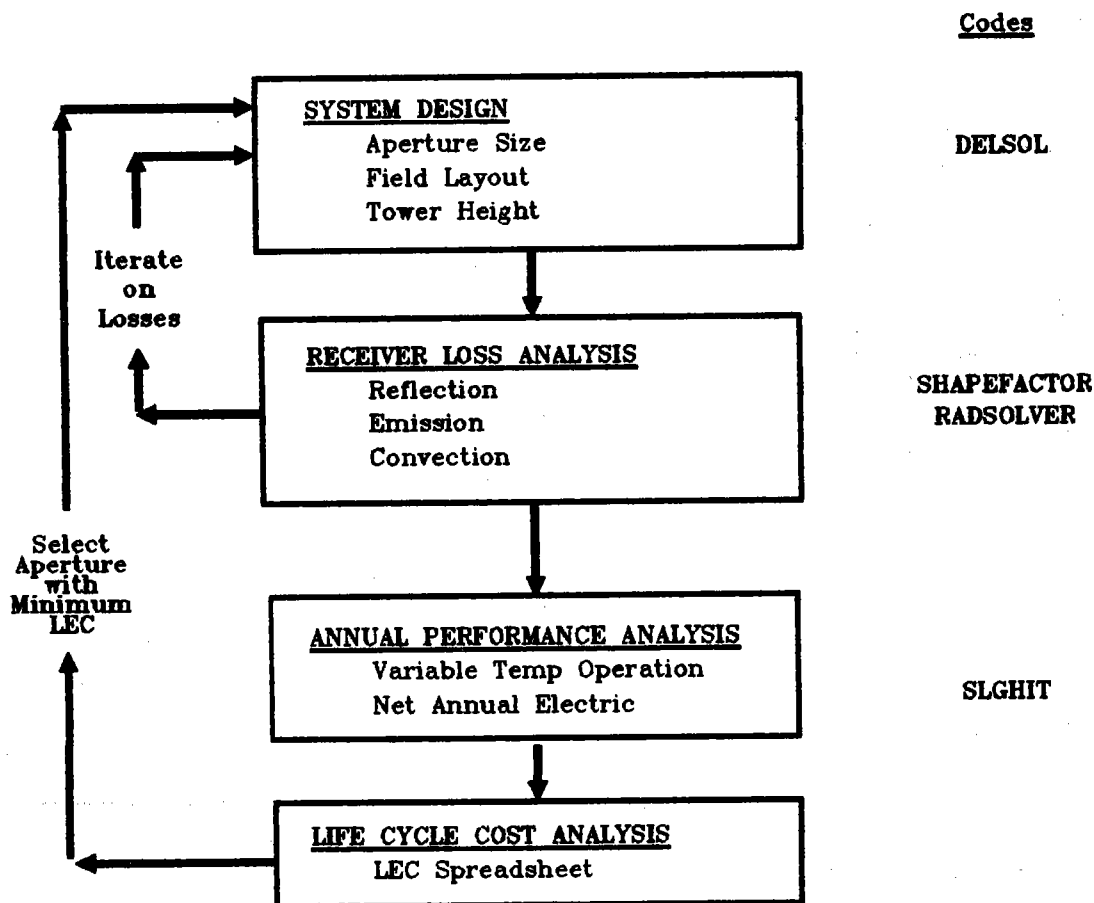


Figure 3-1. Flowchart of the high-temperature DAR design process

For the high-temperature DAR performance analysis, the novel feature of the approach adopted for this study was to feed back the annual energy prediction results (incorporating variable temperature operation) into the process of selecting optimal receiver aperture size. The implementation of this approach is diagrammed in Figure 3-1. As indicated, performance of the high-temperature DAR system was evaluated over a range of receiver apertures. For each aperture size, a system layout was developed (subject to convergence on thermal loss estimates), annual performance was estimated, and the leveled energy cost was computed. The aperture size producing the lowest leveled energy cost was selected as the representative case.

As mentioned previously, the annual performance model SLGHIT explicitly models variable temperature operation by balancing incident flux, thermal losses, and turbine operating temperature at each time step in the annual energy simulation. Thus, the estimate of annual energy performance accounts for the good part-load performance of the ISTIG engine coupled with improving receiver efficiency at lower temperatures.

Figure 3-2 shows the leveled energy cost versus aperture area results for the high-temperature DAR. The aperture producing the lowest leveled energy cost was 21 m by 16.8 m, and the average receiver outlet temperature was 1165°C. The corresponding field size was 485,400 m². Based on DELSOL design runs for this system, this optimum aperture is about 20% larger than would normally have been selected for a receiver operating at a (fixed design point) temperature of 1320°C. This difference in the optimum aperture size highlights the difference for a variable temperature system between a design based on the rated design conditions and a design based on the annual energy production. In this case, average annual receiver operating temperatures are significantly below the rated operating temperature. Because the lower temperatures produce lower thermal losses, higher annual energy production is achieved by selecting a larger aperture and reducing the optical spillage losses.

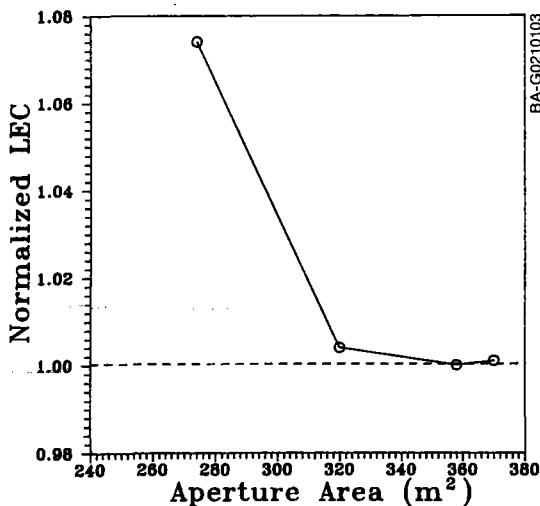


Figure 3-2. Levelized energy cost as a function of aperture area for the high-temperature DAR system. Because of the variable-temperature operation of the system, the optimum aperture had to be determined on the basis of annual performance.

In addition to the general parasitic losses listed above, the high-temperature DAR model also included the receiver loop fluid pumping power.

3.2 Particle Injection Receiver

The design for the PIR system followed a different track from the high-temperature DAR analysis. The PIR design was much more constrained to achieve high flux levels at the receiver aperture to ensure that sufficiently high outlet temperatures would be achieved. Bechtel estimated that they needed flux levels larger than 2.5 MW/m² at the aperture plane to produce the receiver outlet temperatures required when using the AAHX (see Appendix A). The maximum required temperature from the receiver is a strong function of the effectiveness of the heat exchanger interposed between the receiver air loop and the ISTIG engine. As the effectiveness of the heat

exchanger improves, the heat exchanger cost increases and the required receiver temperature decreases. For this reason, the PIR system design focused on minimizing the heat exchanger cost within the bounds of achievable particle temperatures. This analysis resulted in selecting an effectiveness of 0.85 as the optimum.

DELSOL was used to optimize the tower height, aperture size, and field layout subject to the engineering constraints just mentioned. The baseline design resulted in a tower height of 190 m, a field size of 461,100 m² and an aperture size of 18 m by 16 m. In addition to producing an annual field efficiency table for the PIR system, this effort also produced receiver loss estimates and operating performance characteristics using the code 2DPRTS [12]. The code 2DPRTS is a time-dependent, two-flux model. It accounts for absorption, scattering, and emissive radiative transfer as well as convection heat transfer within the particle cloud. Receiver convection losses per se were not modeled but were treated in the context of makeup flows for the air curtain used in the PIR design.

The receiver losses for the PIR/DCHX system were extrapolated from the PIR system with the AAHX. The replacement of the AAHX with the DCHX leads to lower receiver temperatures and thus lower receiver thermal losses. The extrapolated loss fractions ranged from about 13% to 14% over the range of inputs, which is several percentage points lower than for the PIR system with AAHX. Bechtel has estimated (see Section 5.2 in Appendix A) that because of the design changes possible with the lower required receiver temperature, these values may be conservative and the actual loss fractions may be as low as 10%.

Once the PIR configurations had been established, the annual performance (with variable temperature operation) was modeled with SLGHIT, much as described for the high-temperature DAR. For PIR, the major parasitic losses included the blower power for both the primary airflow through the receiver and for the flow necessary to maintain the air curtain across the receiver aperture.

3.3 Volumetric Receiver

The volumetric receiver system design drew heavily on the results of the more detailed design effort for the high-temperature DAR. In the absence of information about material limitations on the fiber pack, the same flux levels were used for the volumetric receiver as for the high-temperature DAR (0.8 MW/m² average and 1.8 MW/m² peak). Thermal loss estimates for the volumetric receiver were developed from information calculated by Karrais [19] that describes the radiative loss fraction from a unit area of the fiber pack as a function of outlet temperature and incident flux. The loss fraction curves developed from the Karrais data are shown in Figure 3-3.

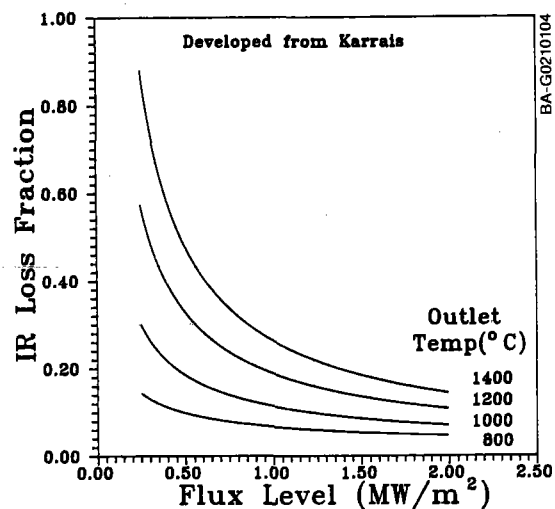


Figure 3-3. Infrared emission loss curves for the volumetric receiver. Adapted from Karrais [19].

The volumetric receiver emissive losses were calculated using (1) the curves in Figure 3-3, (2) a map of incident fluxes, and (3) the receiver outlet temperature. First, the front surface of the fiber pack was divided into small zones roughly a meter on a side. Then, using a flux map generated in DELSOL, the average flux was calculated for each of these zones. Knowing the required outlet temperature and these average flux values, the loss fraction for each zone could be determined from the information developed by Karrais [19] (as in Figure 3-3). Summing the emissive losses for each zone gave the losses for the entire fiber pack.

The reflective losses were estimated using an effective cover ratio (the effective fraction of front surface area occupied by fibers) and the reflectance of the silicon carbide fibers. The inward airflow of the volumetric receiver was assumed to obviate convection losses.

This thermal loss analysis produced results similar in magnitude to the high-temperature DAR for comparable receiver temperatures; thus, similar tower, field, and receiver sizes were used. The aperture width of 21 m, the same as the optimum high-temperature DAR aperture, was selected for analysis for the volumetric receiver system. A field layout and field performance table were generated using DELSOL. As with high-temperature DAR and PIR, the system design results were then used as input to SLGHIT to predict annual energy production.

The Karrais data used here represented the most readily adaptable thermal loss characterization of the volumetric receiver concept available at the time of this study. However, it should be recognized that thermal loss estimates for the volumetric receiver are extrapolations from this data in several instances. For example, this data was generated for temperatures slightly lower than the range evaluated for this study, and the extrapolation to the higher temperatures examined here introduces uncertainty.

The Karrais data is also based on using ambient temperature air as the receiver inlet, as in the VR/amb case. For the VR/tb-ex or volumetric receiver/DCHX cases, where the turbine exhaust stream was returned to the receiver inlet, this assumption is violated. Thus, for these cases the losses derived from this procedure should underpredict the receiver losses.

Finally, the volumetric receiver loss estimates required several assumptions about the geometry of the receiver. For example, it was assumed that there were no additional losses caused by interior structure within the fiber pack. This would be possible if (1) the entire fiber pack were constructed as a single unit with very long fibers or (2) if the framework necessary for constructing the fiber pack from smaller modules did not appreciably increase the reflective and emissive losses.

Recently, Skocypec, Boehm, and Chavez [24] developed a more rigorous model for the volumetric receiver fiber pack heat transfer. Figure 3-4 shows a comparison of the loss fractions developed from the Karrais data (the infrared loss fractions shown in Figure 3-3 plus the reflective loss estimates) with those predicted for a very similar case by Skocypec. These results indicate that the losses estimated here may be too low. However, even this more recent data represents only an initial estimate of the potential performance of the volumetric receiver. In particular, no effort was made to optimize the design of the fiber pack beyond assuring that it behaved in a reasonable fashion (e.g., checking that the highest temperatures did occur near the back of the pack and that the solar and infrared flux profiles looked reasonable).

Clearly, a more comprehensive study of the volumetric receiver performance could be done. However, note that virtually all of the assumptions made here about the volumetric receiver performance have been optimistic and tend to overpredict the performance. In addition, the conclusions about the volumetric receiver in this study are based primarily on comparison with the PIR, which is a direct competitor. Given that the product of each receiver is the same (hot air at atmospheric pressure), their overall results would need to be close before the uncertainties listed here would become critical. We shall see in the next section that this is not the case.

As with the other systems, SLGHIT was used to predict the annual performance over the variable temperature operating range. The parasitic losses unique to the volumetric receiver included the power required to operate the blower that draws air through the fiber pack, the AAHX (or DCHX), and the steam generator.

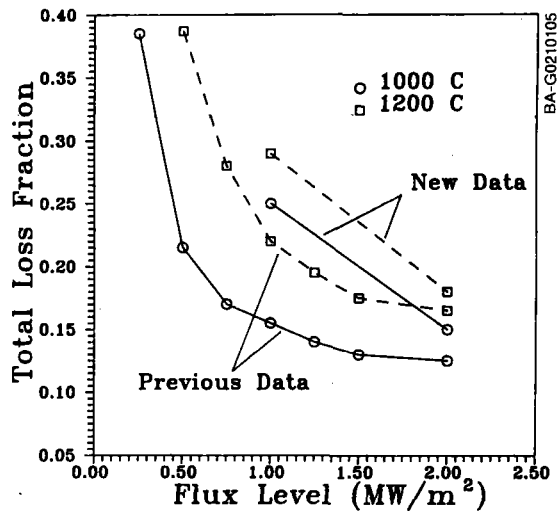


Figure 3-4. Comparison of loss curves from Karrais [19] and Skocypiec, Boehm, and Chavez [24]. The Karrais values were used to generate the results presented here. A later, more rigorous analysis by Skocypiec, Boehm, and Chavez showed that the Karrais values may be optimistic.

4.0 COST ESTIMATES

Accurately estimating the costs of a component or subsystem that has not yet been designed is a difficult proposition at best. The costs presented in this section were developed in two ways. The costs for many of the standard solar central receiver components, such as the heliostats, transport, and balance of plant, were developed from the cost goals published in the U.S. Department of Energy's (DOE) Solar Thermal Technology Program multiyear plan [25]. The other two cost categories, receiver-tower and conversion (often called EPGs, which here includes the heat exchanger), were critical to this analysis and had to be estimated for each system individually.

4.1 Costs from the Cost Goals

Table 4-1 shows the cost goals from the multiyear program plan [25] for all major categories except receiver and conversion. Similarly, Table 4-2 shows the economic parameters required to calculate the levelized energy cost. These parameters were also drawn from the multiyear program plan.

Although the costs are listed in Table 4-1 as a function of field area, several adjustments were made. In the case of the transport costs, the same value was used for all of the high-temperature systems since they all required similar ducting between the engine and the heat exchanger. Similarly, the balance-of-plant costs were assumed to be the same for all of the systems, including the low-temperature DAR. Although this probably penalizes the high-temperature systems somewhat*, it was impossible not to make an arbitrary distinction at this level of detail. Each of these costs represent a small fraction of the overall system cost, and none are likely to affect the results in any significant way.

**Table 4-1. Development of System Capital Costs
Long-Term Goals (Dec 1985)**

System Elements	Costs
Heliostats	\$40/m ² (of heliostat area)
Transport	\$25/m ² (of heliostat area)
Storage	\$20/kWh _{th}
Balance of plant	\$30/m ² (of heliostat area)
Indirects and contingencies ^a	20%

^aThe total capital cost of the system was calculated by summing the costs for the individual components (i.e., the elements from this table plus the receiver and conversion) and increasing that value by 20% to account for indirect costs and contingency factors [25].

*The balance-of-plant costs included buildings, site improvements, master control system, spare parts, and plant service factor. With a simpler plant and everything on the tower-top, the balance-of-plant costs for the high-temperature systems should be smaller than for a salt-steam engine system with storage.

4.2 Receiver and Conversion Costs

Table 4-3 lists the receiver and conversion categories for each system, indicates the author's assessment of the uncertainty level associated with the cost estimate, and describes how the costs were estimated in each case.

It must be noted that a designation of low uncertainty in this ranking should be interpreted as a relative indication. In most cases, this designation means that the item in question is quite similar to an item that is currently available and does not require a substantial advancement from current technology. It does not indicate that the cost is fixed and firm or even that such an item could necessarily be purchased today.

Notice that many of the cost estimates had to be made by analogy to more conventional or near-term technologies, and several of these involved fairly arbitrary factors to account for higher temperatures or general uncertainty. The sensitivity of the results to the most critical values among these, in particular the receiver and DCHX costs, will be examined in the sensitivity analysis.

Because gas turbine technology is generally cheaper than steam-Rankine, the \$420/kW_e cost shown for the ISTIG engine seems about the right magnitude when compared with the \$650/kW_e Rankine cycle cost. However, the cost of the AAHX for the volumetric receiver and the PIR increases the total conversion cost to \$770/kW_e (= \$420/kW_e + \$38.6M/110 MW_e). By contrast, the high-temperature DAR, using a DCHX at \$4M, has a total conversion cost of only \$456/kW_e, still well below the cost of the Rankine conversion equipment.

The relative costs of these various categories for each system are shown in the bar chart in Figure 4-1 where the transport and balance-of-plant costs (which do not vary between the high-temperature systems) have been omitted for clarity. The heliostat costs reflect the size of the heliostat field required to deliver rated power to the engine at the design point. This was largely determined by the receiver losses and by factors like the exhaust losses described for the volumetric receiver and PIR.

In the cost categories used here, the tower cost is included in the receiver cost. For example, the difference between the receiver costs of the various volumetric receiver systems is caused by the cost of the tower. As the system becomes less efficient, the field size must increase, and in order to maintain the optical efficiency, the tower height must also increase.

The cost estimate for the high-temperature DAR is larger than those for the volumetric receiver and PIR by factors of about 3 and 8, respectively. This probably represents some conservatism in judging the difficulty of containing and pumping the high-temperature liquid. By contrast, the PIR receiver cost reflects the very simple structure and conventional kind of components (e.g., exhaust fans) required by that concept.

The conversion cost is the single largest cost category for all systems, and in the high-temperature systems it completely dominates the total cost. The conversion bars for the

Table 4-2. Levelized Energy Cost Economic Scenario Assumptions (Real dollars, excludes inflation)

Discount rate	0.0315
Fixed charge rate	0.0593
Capital recovery factor	0.0520
Construction time adjustment factor	1.0318

Table 4-3. Source of Cost Estimates for the Receiver and Conversion Cost Categories

Receiver Costs

High-Temperature DAR: \$26M (uncertainty: high)

Based on the cost of a low-temperature DAR (\$6.5M) as estimated by Solar Power Engineering Company, Inc., in Anderson et al. [10]. An arbitrary factor of four was included to account for the increased cost of high-temperature materials required for fluid pumping and containment.

PIR: \$2.7M (uncertainty: low)

Estimated by Bechtel (see Appendix A) based on engineering study and vendor quotes

Volumetric Receiver: \$8.0M (uncertainty: high)

Based on the cost estimate from Pacific Northwest Laboratories [13]. Adjusted according to differences in physical size (e.g. number of fibers, size of backing surface), not adjusted for temperature.

Tower: (uncertainty: low)

Based on cost algorithm from DELSOL. Although some uncertainty is introduced by the weight of the engine and heat exchanger, this will not require a major advancement of the technology.

Conversion and Heat Exchanger

ISTIG engine: \$420/kW_e (uncertainty: low)

Estimated by PG&E for Garrett [26]

Rankine engine: \$650/kW_e (uncertainty: low)

"Current technology" value from the multiyear program plan [25] (to compare with the "current" value for the ISTIG)

AAHX: \$38.6M (uncertainty: low)

Estimated by Bechtel, based on vendor quotes for today's technology. (No adjustments were made for future improvements.)

DCHX: \$4M (uncertainty: high)

Based on the cost of a DCHX for carbonate salts at 900°C (about \$1M), which was estimated from a procedure outlined by Bohn [15]. An arbitrary factor of 4 was applied to account for the increased cost of high-temperature pumping and containment materials.

high-temperature systems in Figure 4-1 are divided so the bottom portion represents the cost of the ISTIG engine and the upper portion is the cost of the heat exchanger. Notice that the cost of the AAHX roughly doubles the cost of conversion for the volumetric receiver and PIR. The conversion cost for the low-temperature DAR is relatively small despite the larger cost per kW_e because the storage system allowed the use of a smaller engine than was possible with the high-temperature systems.

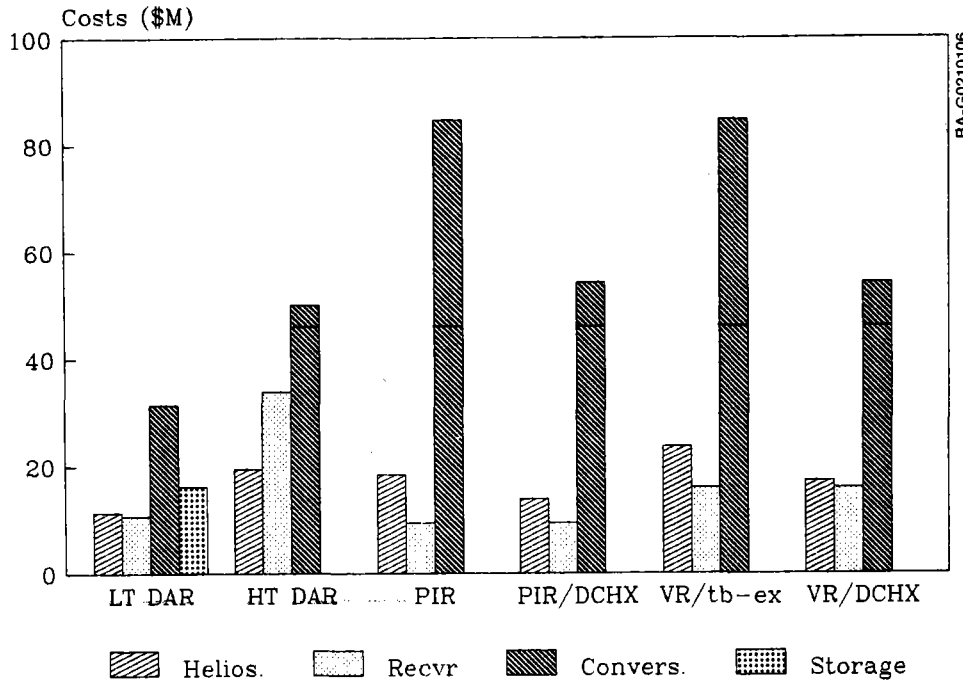


Figure 4-1. Breakdown of the system capital costs by subsystem. The lines through the conversion bars divide the cost of the ISTIG engine (bottom) from the cost of the heat exchangers (top). The transport and balance-of-plant costs are common to all the high-temperature systems and were omitted from this graph for clarity.

5.0 RESULTS

5.1 Performance Results

Figure 5-1 shows the overall annual thermal-to-electricity efficiency for all of the cases studied. The PIR/DCHX at 25% has by far the largest annual efficiency. The high-temperature DAR system, the PIR system, and the volumetric receiver/DCHX system all fall within the annual efficiency range of from 18% to 20% and are very competitive with the low-temperature DAR. However, because of the larger receiver losses and higher exhaust temperatures, the overall annual efficiency of the VR/tb-ex case is only 14%.

The annual efficiencies for each system are broken down into subsystem efficiencies in Figure 5-2. In this figure the subsystem efficiencies are presented in cumulative fashion (sometimes called a waterfall efficiency chart) so the length of each of the bars represents the product of all of the efficiencies before it. For example, the first bar represents the annual efficiency of the heliostat field, and the second bar includes the efficiency of both the heliostat field and the receiver. The exhaust losses are defined as the energy lost when the exhaust stream is at a temperature above the exhaust temperature of the original ISTIG engine. The category labeled storage losses describes the efficiency of the storage and piping system and is significant only for the low-temperature DAR case. The decrease in efficiency between the conversion bar and the overall bar is caused by energy lost during startups and by parasitic losses.

All of the high-temperature systems have significantly lower field efficiencies than the low-temperature DAR system. This is because they have larger heliostat fields and concomitantly more spillage and attenuation.

The decrease in receiver performance between the low-temperature DAR and the high-temperature DAR (caused by the increased losses at higher temperatures) can be seen clearly. By contrast, because of the efficient absorption of the very small particles, the PIR efficiency is nearly as good as the low-temperature DAR, which operates at a temperature about 700°C lower.

The decrease in exhaust losses in going from the VR/tb-ex to the volumetric receiver/DCHX is very clear. Although these losses are to some extent an artifact of the limitations of this study, to some extent they also represent true design and operational problems that might be faced by the volumetric receiver system. For example, there will be some limit on how much steam can be injected into the ISTIG engine, and this will limit how much of the extra exhaust enthalpy can be used. It is also not clear that it will be possible to inject the turbine exhaust stream directly into the volumetric receiver absorber pack without either diluting it with ambient air or adding some kind of window over the aperture, either of which would result in a loss of performance. Note that the volumetric receiver/DCHX case takes advantage of all of the possible benefits: the losses are based on ambient inlet air, but the reduced heating requirements are based on turbine exhaust inlet air and direct-contact heat exchange.

All of the volumetric receiver systems suffer by comparison to the PIR, especially when combined with the DCHX. The moderate scattering losses, and particularly the low emission losses of the very small particles in the PIR, are extremely beneficial at these high temperatures. Overall, the PIR appears to have a marked performance advantage over the volumetric receiver.

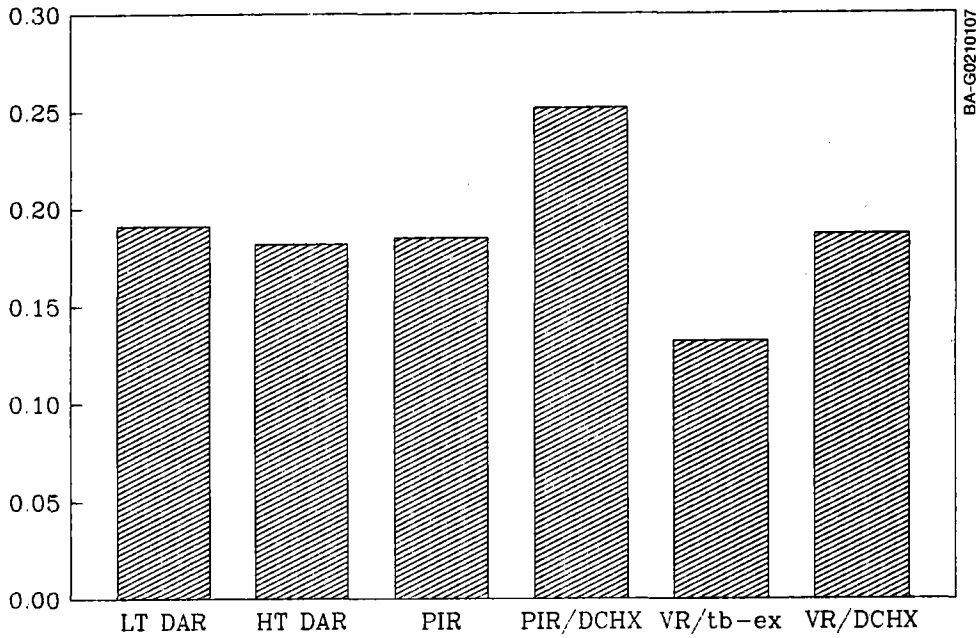


Figure 5-1. Annual thermal-to-electricity efficiency from insolation incident on the heliostats to net electricity

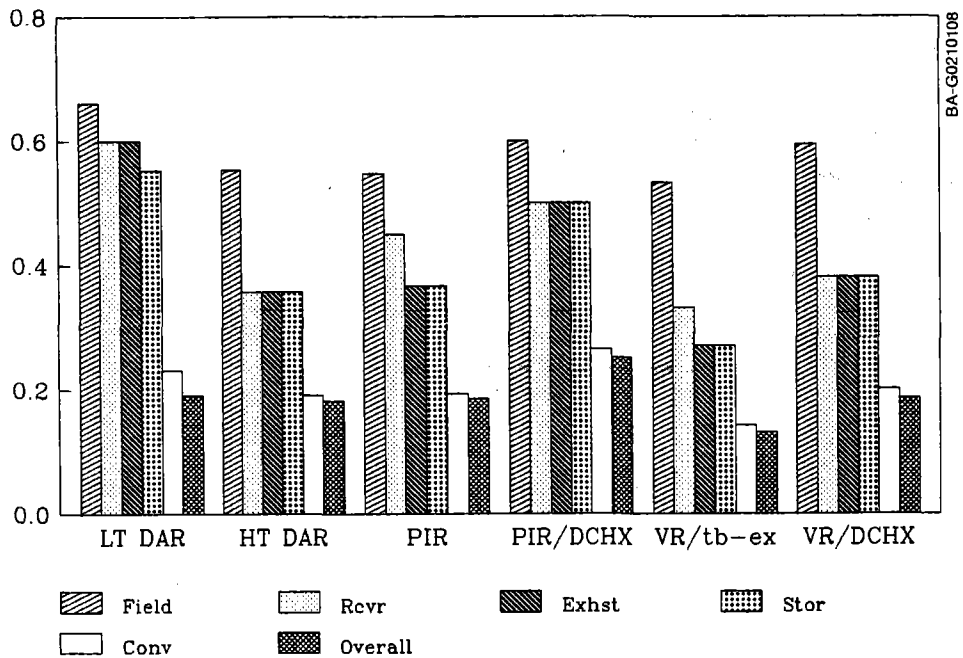


Figure 5-2. Cumulative subsystem efficiency bar charts (waterfall charts) for all of the systems

Because of the good part-load performance of the ISTIG engine, the annual conversion efficiency is about 52%-53% for all of the high-temperature systems. This is in contrast to the roughly 40% efficiency for the low-temperature DAR Rankine system.

5.2 Levelized Energy Cost

The figure of merit ultimately used to compare the various systems is the levelized energy cost, which is shown for each system in Figures 5-3a and 5-3b. In general, several of the systems were quite competitive with both the low-temperature DAR (the normalizing case for Figure 5-3b) and the Solar Thermal Technology Program cost goal of \$0.05/kWh. In particular, the high-temperature DAR, the PIR with the AAHX, and the volumetric receiver/DCHX cases all are within a few percentage points of the levelized energy cost for the low-temperature DAR. The only clear stand-out is the PIR/DCHX, which produced a levelized energy cost almost 30% lower than that of the low-temperature DAR. As noted in Section 2.4, the PIR/DCHX case is probably somewhat conservative insofar as it uses receiver losses extrapolated from the higher temperature PIR/AAHX case.

There are two factors not explicitly accounted for in the levelized energy cost values shown here. The first is the cost of the fuel consumed by the PIR in making the particles. About 13,567 barrels of fuel oil would be required annually, which at \$20/bbl would result in a cost of only \$271,341 (or about \$0.001/kWh). The second factor not explicitly accounted for is the water consumed to make the steam for the ISTIG process. The amount of water consumed is on the order 39 million gallons per year; the cost of this water will depend on the plant location.

Because of the uncertainty associated with several of the cost values, the sensitivity of the results to several of the cost assumptions was examined. The first of these cost assumptions was the heliostat cost. The heliostat cost listed in the long-term goals (\$40/m²) is quite low, and when compared with the higher values for the conversion equipment, might tend to underemphasize the value of thermal performance. Figure 5-4 shows the effect of increasing the heliostat cost to \$100/m² for all of the systems including the low-temperature DAR (it was assumed that all systems would have access to the same concentrator technology). In this plot all of the levelized energy cost values were normalized to the low-temperature DAR case independently for each heliostat cost. It is clear that the changes in the capital costs caused by the increased heliostat cost do not change the relative results significantly.

Another element with a substantial uncertainty is the high-temperature DAR cost. The effect of perturbations in this value is demonstrated in Figure 5-5 where the high-temperature DAR cost is varied about its base value of 4 times the low-temperature DAR cost. It can be seen that when the high-temperature DAR cost is reduced to half as much as the base case (from \$26M to \$13M), then the high-temperature DAR levelized energy cost would be about 13% lower than the low-temperature DAR. Similarly, if the cost of the high-temperature DAR were increased by a factor of 2.5 above the base high-temperature DAR case (to \$65M), then the levelized energy cost for the high-temperature DAR would be about 14% larger than that of the low-temperature DAR. Because the high-temperature DAR would continue to be roughly competitive with the low-temperature DAR, even at the highest cost, the relative results appear largely insensitive to these changes.

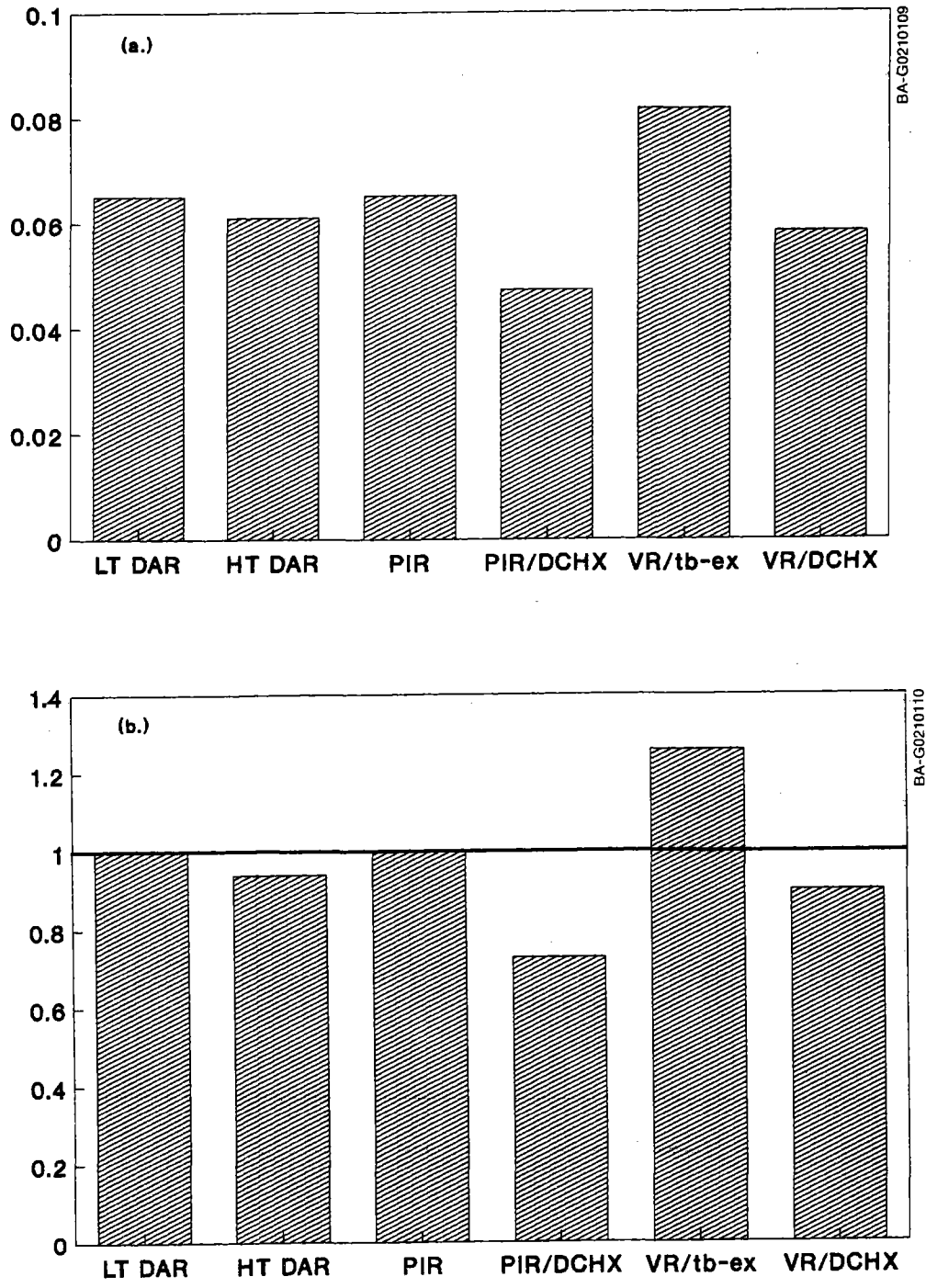


Figure 5-3. Levelized energy costs: (a) values in $\$/kW_e$ and (b) values normalized to that of the low-temperature DAR system. The levelized energy cost for the PIR/DCHX is nearly 30% lower than that of the low-temperature DAR.

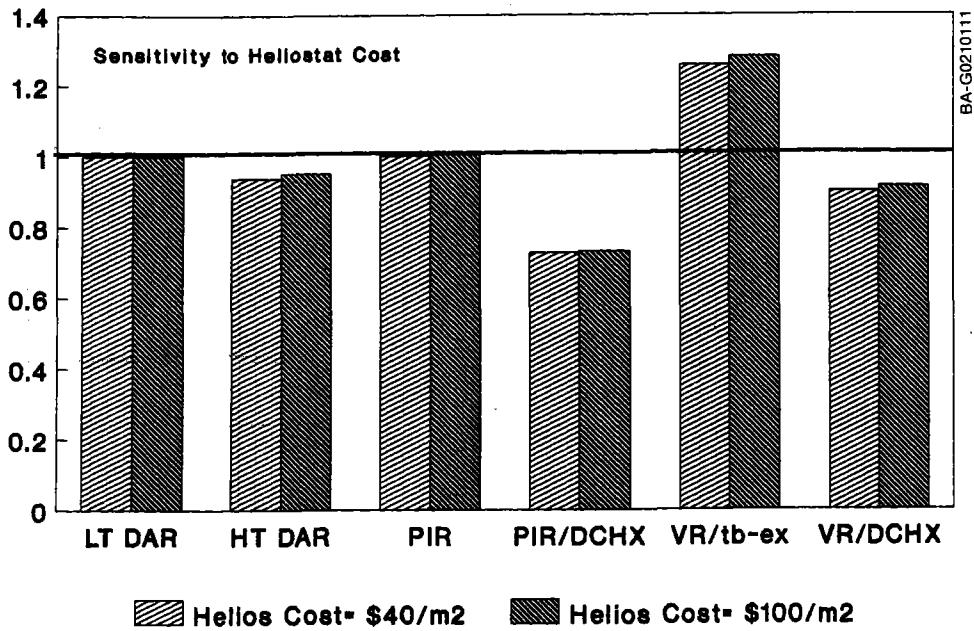


Figure 5-4. Sensitivity of the levelized energy cost results to increased heliostat costs. The baseline heliostat cost was \$40/m². Increasing this component cost to \$100/m² does not change the relative standings.

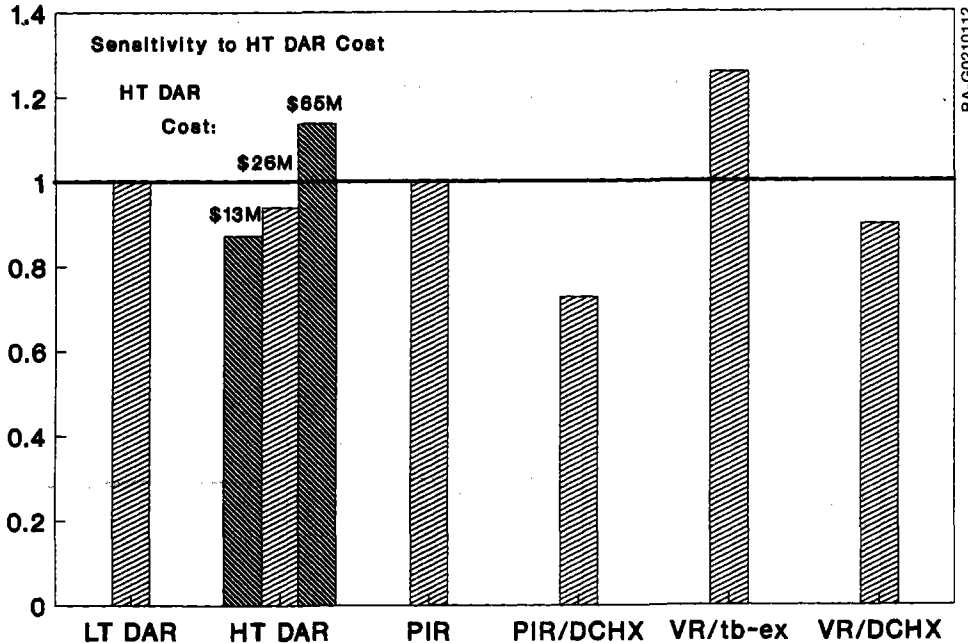


Figure 5-5. Sensitivity of the levelized energy cost results to the cost of the high-temperature DAR. The baseline receiver cost was about \$26M. The levelized energy cost was also calculated for receiver costs of \$13M and \$65M. Over this range of receiver costs, the conclusions would not change significantly.

There is also a large uncertainty associated with the cost of the volumetric receiver. However, (as with the high-temperature DAR) reducing the cost of the volumetric receiver by a factor of 4 (to \$2M from roughly \$8M) changes the levelized energy cost only slightly and does not change the conclusions at all.

Because the performance of the DCHX has such a large effect on the levelized energy cost results for the PIR and volumetric receiver systems, the sensitivity of the results to this cost was also examined. Figure 5-6 shows the effect of assuming that each DCHX (with a base case cost of about \$4M) costs half as much as the AAHX (i.e., about \$19M apiece), so the PIR/DCHX and volumetric receiver/DCHX systems (which use two DCHXs) have the same conversion cost as the corresponding cases with the AAHX. Even in this rather severe case, the PIR/DCHX still shows a better than 10% improvement in levelized energy cost over the low-temperature DAR.

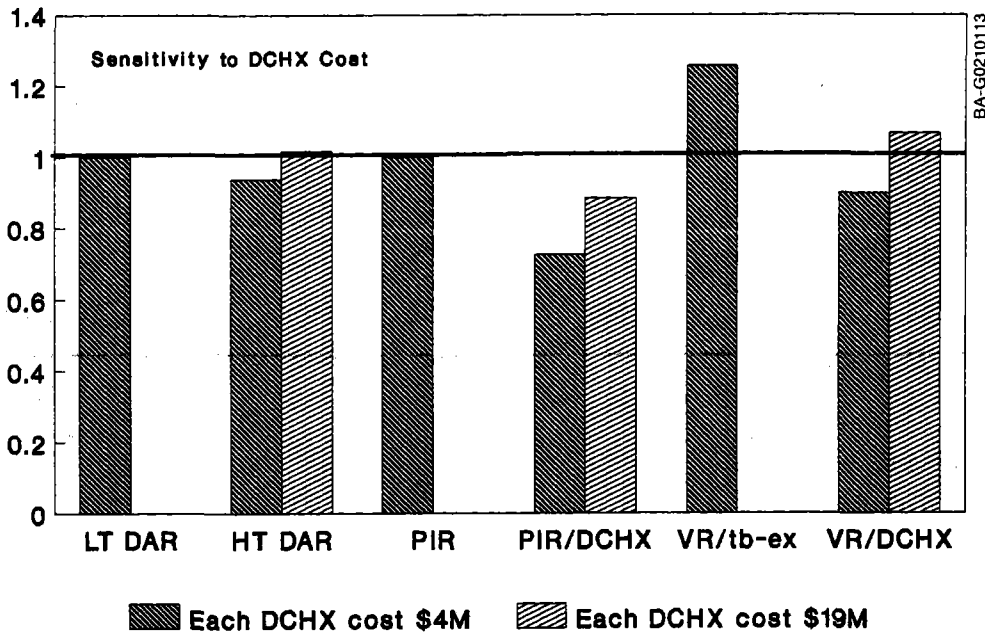


Figure 5-6. Sensitivity of the levelized energy cost results to the cost of the DCHX. The base cost was \$4M. Increasing that cost to \$19M does not significantly change the results. Note that the PIR/DCHX and the volumetric receiver/DCHX systems use two DCHXs apiece and therefore show heat exchanger costs of \$8M and \$38M.

6.0 CONCLUSIONS AND RECOMMENDATIONS

6.1 Conclusions

Based on the results listed in the previous section and subject to the assumptions and caveats listed earlier, the following conclusions appear to be valid:

- None of the systems listed here is likely to be viable in the very near term. Even the fossil-fired ISTIG engine — the system element most likely to be developed in the near term — is by no means a certainty, and there are currently no plans that the authors are aware of to develop an externally fired version of this engine.
- The combination of a very high-efficiency engine and advanced receiver does appear to have the potential to be competitive with the low-temperature (550°C) technology. The best case examined here, the PIR/DCHX, produced a levelized energy cost nearly 30% lower than the low-temperature DAR, although it required substantial advancements in two technological areas.
- Of the system concepts examined in this effort, the PIR appears to have performance and cost advantages over the volumetric receiver and the high-temperature DAR at these temperatures (1350°C). This conclusion is based on admittedly poor receiver loss estimates for the volumetric receiver. However, it seems supportable in light of the very good performance and extremely low cost estimates for the PIR. Since both receivers supply hot atmospheric-pressure air, the volumetric receiver would have to demonstrate significant performance improvements, cost improvements, or both to compete successfully.
- The DCHX appears to have the potential to be a major contributor to a successful high-temperature system. The DCHX should be able to:
 - lower receiver temperatures and thus improve performance
 - lower capital costs
 - provide the potential for liquid storage in air heating systems.

A high temperature DCHX will be critical to the development of a successful high-temperature DAR system and will substantially improve the capital cost and levelized energy cost of the PIR system.

Overall, the results of this effort are significantly more encouraging than many previous high-temperature electricity generation studies. It seems probable that as technology advances, the trend in power generation will be toward higher temperatures and improvements in materials, which may continue to make high-temperature central receiver systems more attractive.

6.2 Recommendations

To reap the full benefits of high-temperature electricity systems, several areas of technological uncertainty should be addressed. Addressing these issues will result in a better understanding of the basic phenomena involved in using high-temperature heat transfer and highly concentrated flux. In addition to the benefits these activities provide for high-temperature electricity production, other studies [27] indicate that they may also be useful in other than electricity applications of concentrated solar flux, particularly solar chemical reactions, which are driven by higher temperatures beyond today's receiver technology. Thus, these recommended actions could provide even a larger payoff than is immediately obvious:

- Continue DCHX research. The results of the analysis presented here have demonstrated the potential importance of this component. If the survey of potential fluids identifies one or more strong candidates, then some of the emphasis in the DCHX work can be shifted to high-temperature systems.
- Examine the particle and fluid mechanics issues associated with the PIR in a preliminary way. For example, the bulk particle radiative characteristics and chemical kinetics could be studied in laboratory-scale experiments, and a literature search and analytical efforts could be directed to the issue of controlling high-temperature, high-speed air flows over large areas.
- Continue efforts directed at developing better analytical loss estimates for the volumetric receiver fiber pack. This will not require a major effort but will tell us whether the volumetric receiver performance is better than estimated here to warrant further investigation as a source of high-temperature air.
- Conduct a preliminary survey for a high-temperature working fluid for the high-temperature DAR or for a high-temperature DCHX. Again a modest effort could provide a significant improvement in understanding how difficult it will be to identify this important element. For example, if there are a number of candidates that are fairly cheap, readily available, and do not have major materials compatibility problems, then the probability of finding an acceptable fluid can be judged to be fairly high.
- Track the development of ISTIG and other advanced high-efficiency engines. It appears likely that the development of the fossil-fired versions of these engines will occur without assistance from the Solar Thermal Technology Program. However, development of externally fired engines may require DOE incentives.

It is felt that the accomplishment of these tasks in the near term will give a better sense of the accuracy of the assessments made in this current effort and of the degree of difficulty involved in bringing the various technologies to fruition.

6.3 Technical Uncertainties

As pointed out earlier in the text, many of the components examined here have important technological areas in which research and development is needed. However, not all of these areas will require the same amount of research and development effort. Although it was beyond the scope of this study to attempt to estimate either the funding levels required or the probability of success for the competing technologies, a qualitative assessment was made. The results of this assessment are given in Appendix B. It is hoped that the reader can use the data given in this appendix as a starting point for a more detailed assessment.

7.0 REFERENCES

1. Lewandowski, A., et al., Direct Absorption Receiver System Study, Phase 1: A Status Report Prepared Under Task 5101.31, SERI/SP-253-2438, Golden, CO: Solar Energy Research Institute, July 1984.
2. Lewandowski, A., et al., Direct Absorption Receiver System Study, Phase 2: A Status Report Prepared under Task 5101.31, SERI/SP-253-2592, Golden, CO: Solar Energy Research Institute, December 1984.
3. DeLaquil, P., C. L. Yang, and J. E. Noring, Solar Central Receiver High Temperature Process Air Systems, SAND82-8254, Livermore, CA: Sandia National Laboratories, February 1983.
4. Bird, S. P., et al., Evaluation of Solar Air-Heating Central Receiver Concepts, PNL-4003, Richmond, WA: Pacific Northwest Laboratory, June 1982.
5. DeLaquil, P., and J. V. Anderson, The Performance of High-Temperature Central Receiver Systems, SAND84-8233, Livermore, CA: Sandia National Laboratories, July 1984.
6. Brown, D. R., L. L. Fassbender, A., and D. Chockie, The Value of Solar Thermal Industrial Process Heat, PNL-5629, Richmond, WA: Pacific Northwest Laboratory, March 1986.
7. Pacific Gas and Electric Company, Scoping Study: LM5000 Steam-Injected Gas Turbine, San Francisco, CA: PG&E, June 1984.
8. Burnham, J. B., M. H. Giuliany, and D. J. Moeller, "Development, Installation and Operating Results of a Steam Injection System (STIG) in a General Electric LM5000 Gas Generator," ASME, 86-GT-231, presented at the International Gas Turbine Conference and Exhibit, Dusseldorf, Federal Republic of Germany, June 1986.
9. Gelfand, Lewis, General Electric Engine Programs, personal communication, 1987.
10. Anderson, J. V., W. Short, T. J. Wendelin, and N. Weaver, Direct Absorption Receiver Systems Assessment, SERI/TR-253-3080, Golden, CO: Solar Energy Research Institute, November 1986.
11. Bohn, M. S., et al., Direct Absorption Receiver Experiments and Concept Feasibility, SERI/TR-252-2884, Golden, CO: Solar Energy Research Institute, October 1986.
12. Schoenung, S. M., P. DeLaquil III, and R. J. Loyd, "Particle Suspension Heat Transfer in a Solar Central Receiver," Solar Engineering - 1987, Proceedings of the 1987 ASME Solar Division Conference, March 1987.
13. Drost, K., Analysis and Design of the Volumetric Air Heating Receiver, SAND84-8190, Livermore, CA: Sandia National Laboratories, July 1985.
14. Kochendorfer, R., and W. Pritzdow, The Volumetric Ceramic Receiver, presented at International Energy Association Meeting, Albuquerque, NM, April 1987, Stuttgart, Germany: Institute for Structures and Design, DFVLR, February 1987.

15. Bohn, M. S., Air/Molten Salt Direct-Contact Heat-Transfer Experiment and Economic Analysis, SERI/TR-252-2015, Golden, CO: Solar Energy Research Institute, November 1983.
16. Maru, H. C., J. F. Dullea, A. Kardas, and L. Paul, Molten Salt Thermal Energy Storage Systems: Salt Selection; Project 8981 Final Report, COO-2888-3, NASA CR135419, Chicago, IL: Institute of Gas Technology, March 1978.
17. Hunt, A. J., and Evans, D. B., Design and Construction of a High-Temperature Gas Receiver Utilizing Small Particles as the Heat Exchanger (SPHER) Phase I Report, LBL-13755, Berkeley, CA: Lawrence Berkeley Laboratory, 1981.
18. Bohren, C. F., and D. R. Huffman, Absorption and Scattering of Light by Small Particles, New York: Wiley-Interscience, 1983.
19. Karrais, B., "Ultralight Modular Ceramic High-Flux Receiver," Solar Thermal Central Receiver Systems, Proceedings of the Third International Workshop, Vol. 2, Konstanz, Federal Republic of Germany, June 1986.
20. Dellin, T. A., et al., A User's Manual for DELSOL2: A Computer Code for Calculating the Optical Performance and Optimal System Design for Solar Thermal Central Receiver Plants, SAND81-8237, Livermore, CA: Sandia National Laboratories, August 1981.
21. Stoddard, M. C., S. E. Faas, C. S. Chaing, and J. Dirks, SOLERGY — A Code for Predicting Annual Energy Production from Solar Central Receivers, SAND86-8060, Livermore, CA: Sandia National Laboratories, May 1987.
22. D. L. Siebers, and J. S. Kraabel, Estimating Convective Energy Losses from Solar Central Receivers, SAND84-8717, Livermore, CA: Sandia National Laboratories, April 1984.
23. Abrams, M., RADSOLVER — A Computer Program for Calculating Spectrally Dependent Radiative Heat Transfer in Solar Cavity Receivers, SAND81-8248, Livermore, CA: Sandia National Laboratories, October 1980.
24. Skocypec, R. D., Boehm, R. F., and Chavez, J. M., "Heat Transfer Modeling of the IEA Volumetric Receiver," presented at the AIChE 23rd National Heat Transfer Conference, 1988. (The data shown in Figure 3-4 are from a personal communication with the authors.)
25. Sandia National Laboratories, National Solar Thermal Technology Program — Five Year Research and Development Plan 1985-1989, Livermore, CA: SNL, December 1985.
26. Garrett Airesearch Manufacturing Company, Conceptual Design Study — Solar Components for a Steam Injected Gas Turbine Solar-Electric Power Plant, 85-21779, San Francisco, CA: Pacific Gas and Electric Company, January 1986.
27. Solar Energy for High Temperature Technology and Applications, Köln, Federal Republic of Germany: DFVLR, 1987.

SERIO 

APPENDIX A

**Analysis of the Particle Injection Receiver
For a 110-MW_e ISTIG Plant**

Bechtel National, Inc.

SERIO 

ANALYSIS OF THE PARTICLE INJECTION RECEIVER

FOR A 110 MWe ISTIG PLANT

PREPARED FOR SOLAR ENERGY RESEARCH INSTITUTE

SUBCONTRACT NO. HX-7-07065-1

P. De Laquil III

S. M. Schoenung

S. M. Patel

Research and Development

Bechtel National, Inc.

July 1987

SERIO 

**ANALYSIS OF THE PARTICLE
INJECTION RECEIVER FOR A 110 MWe ISTIG PLANT**

1.0 SUMMARY

This report presents analyses performed by Bechtel National, Inc. (Bechtel) for Solar Energy Research Institute (SERI) in support of an assessment of high temperature solar central receiver concepts. A 110 MWe intercooled, steam-injected, gas-turbine power cycle was selected by SERI for the assessment because of its high thermal-to-electric conversion efficiency. Design, cost and performance information are provided for the particle injection receiver concept, which is being developed at Bechtel under internal funding. Results of these analyses of the particle injection receiver are summarized as follows:

- The receiver can achieve the necessary design outlet temperature (1480°C) at a receiver efficiency of 85%.
- The receiver operates efficiently at the part load conditions of 75, 50 and 25 percent.
- Electric parasitic loads for the receiver and power cycle are quite small (1.2%).
- The high cost of the ceramic heat exchanger (based upon today's ceramic technology and manufacturing techniques) drives the system design and cost.
- Potential less costly heat exchange approaches should be investigated.

2.0 INTRODUCTION AND SCOPE OF WORK

Several direct absorption solar central receiver concepts have been proposed for electrical generating applications. One of these, the particle injection receiver (PIR) has been under study at Bechtel National, Inc. over the last two years. This concept is a windowless air heating receiver which uses submicron-sized carbon particles suspended in the air stream as the heat absorbing material. Results of a Bechtel-funded feasibility study (Ref. 1) have shown it to be compact and

very efficient, relative to other high temperature central receiver concepts.

The objective of the work described here was to provide design, cost and performance data for the PIR concept to be used in a comparison with other high temperature receiver concepts. Each concept was incorporated into an intercooled steam-injected gas turbine (ISTIG) electric generating cycle. Parameters for the GE LM5000 (110 MWe) ISTIG cycle were selected for use in this study (Ref. 2). The PIR-ISTIG plant is shown schematically in Figure 1.

Our specific work scope items included:

- Cycle Analysis, to determine receiver and heat exchanger thermal requirements
- Receiver Energy Analysis, to determine the collector field and heat absorption region design parameters
- Cost and performance estimate of systems components specific to the PIR concept.

The intercooler, steam generator and compressor-turbine-generator set were assumed to be similar for all the receiver concepts being assessed by SERI, and neither conceptual design nor costing were included in the Bechtel scope of work.

The collector field was designed using 2nd generation, glass/metal heliostats (58.5m^2) as specified by SERI, with a total reflected beam error of 5.2 milliradians in both the horizontal and vertical directions. A sensitivity analysis was performed to determine the impact of using 150m^2 stressed-membrane heliostats with a total reflected beam error of 1.75 milliradians.

Receiver performance was calculated at loads of 100%, 75%, 50% and 25%, to insure that calculations of the plant annual energy generation correctly included the impact of system operation during periods of reduced solar input.

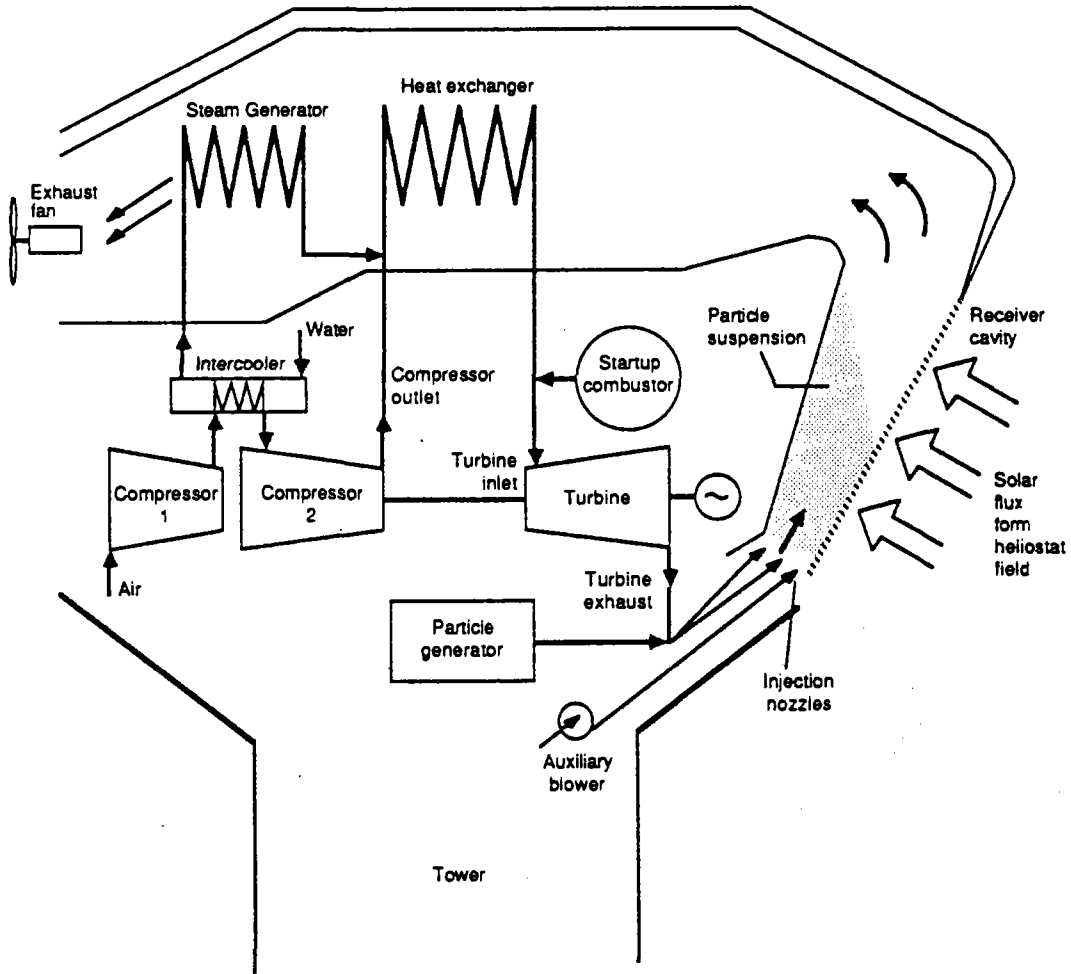


Figure 1 Particle Injection Receiver – Schematic Diagram

3.0 THERMODYNAMIC CYCLE ANALYSIS

A thermodynamic cycle diagram for the PIR-ISTIG cycle is shown in Figure 2. Design point flow rates, temperatures, and pressures for the compressor-turbine cycle components were derived by SERI from the GE report on the LM5000 ISTIG cycle. Fluid conditions for the heat absorption region (velocity, flow rate, temperature) and the hot side of the ceramic/metal heat exchanger (Q_{in} , temperatures) were calculated for the selected power levels. The results were found to be strongly dependent on the heat exchanger effectiveness. Figure 3 shows the relationship between the thermal power to the turbine and the receiver absorbed power for values of the heat exchanger effectiveness ranging from 0.8 to 0.95.

Selection of the optimum design point heat exchanger effectiveness was made by attempting to minimize system cost while still requiring achievable particle suspension temperatures. The major variants in the system cost are the collector field and the ceramic heat exchanger. At low heat exchanger effectiveness, the heat exchanger is small and relatively inexpensive, but the required thermal input (the receiver absorbed power) is significantly greater than the thermal input to the turbine, as indicated in Figure 3. Thus, the collector field is more expensive. In addition, at low heat exchanger effectiveness, the required receiver temperature is significantly greater than the turbine inlet temperature. Thus, a higher receiver flux concentration and particles of low reactivity are required to reach the required receiver temperature.

Figure 4 shows the collector and heat exchanger costs as a function of the heat exchanger effectiveness. The installed collector field cost was given as $91.2 \text{ \$/m}^2$ and the heat exchanger costs are representative of today's technology and today's manufacturing costs. As can be seen in Figure 4, the minimum system cost occurs at an effectiveness of 0.80 or less. However, as can also be seen in the figure, the required receiver temperature is 1540°C . Because the maximum temperature that was

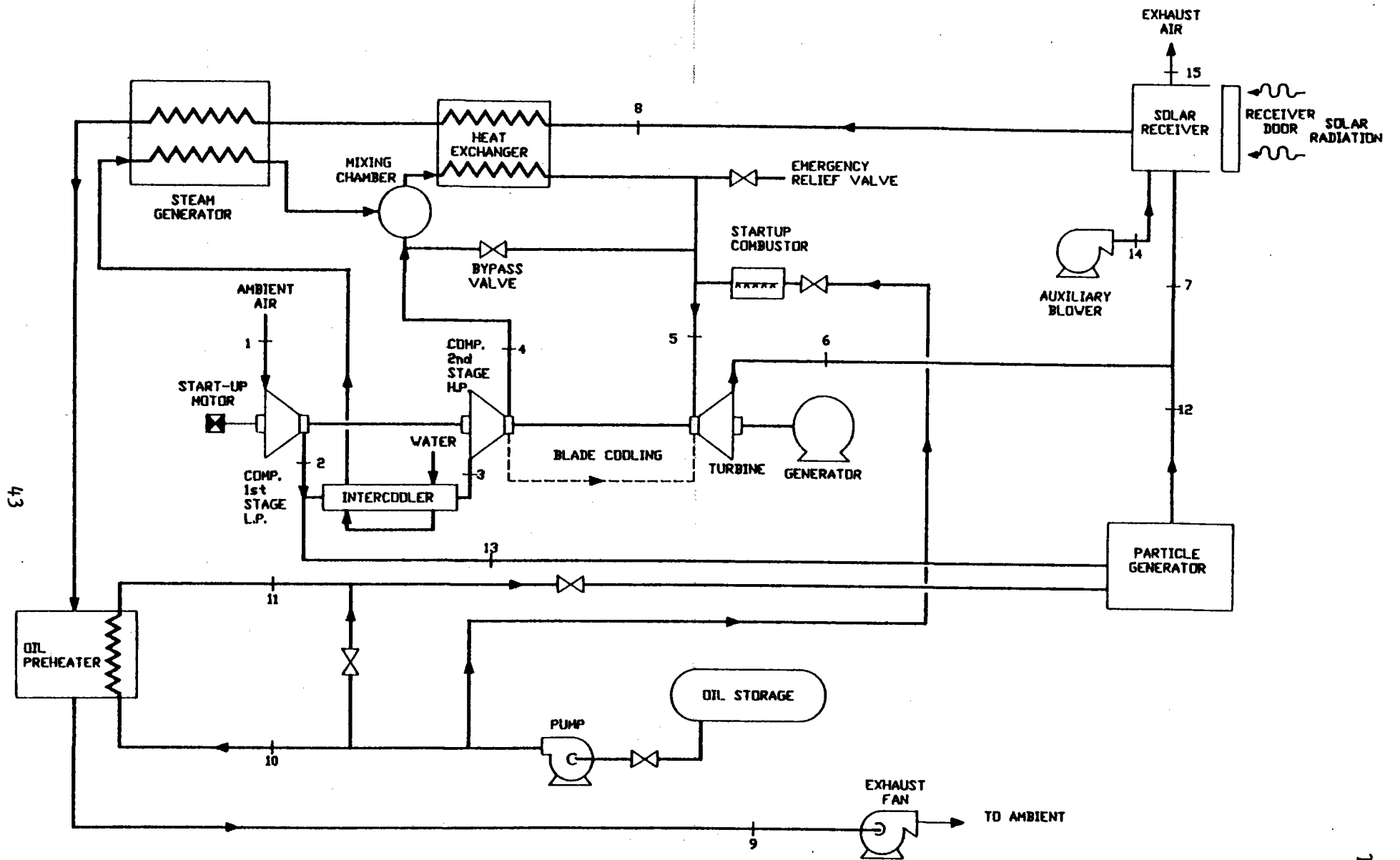


Figure 2 SYSTEM THERMODYNAMIC CYCLE

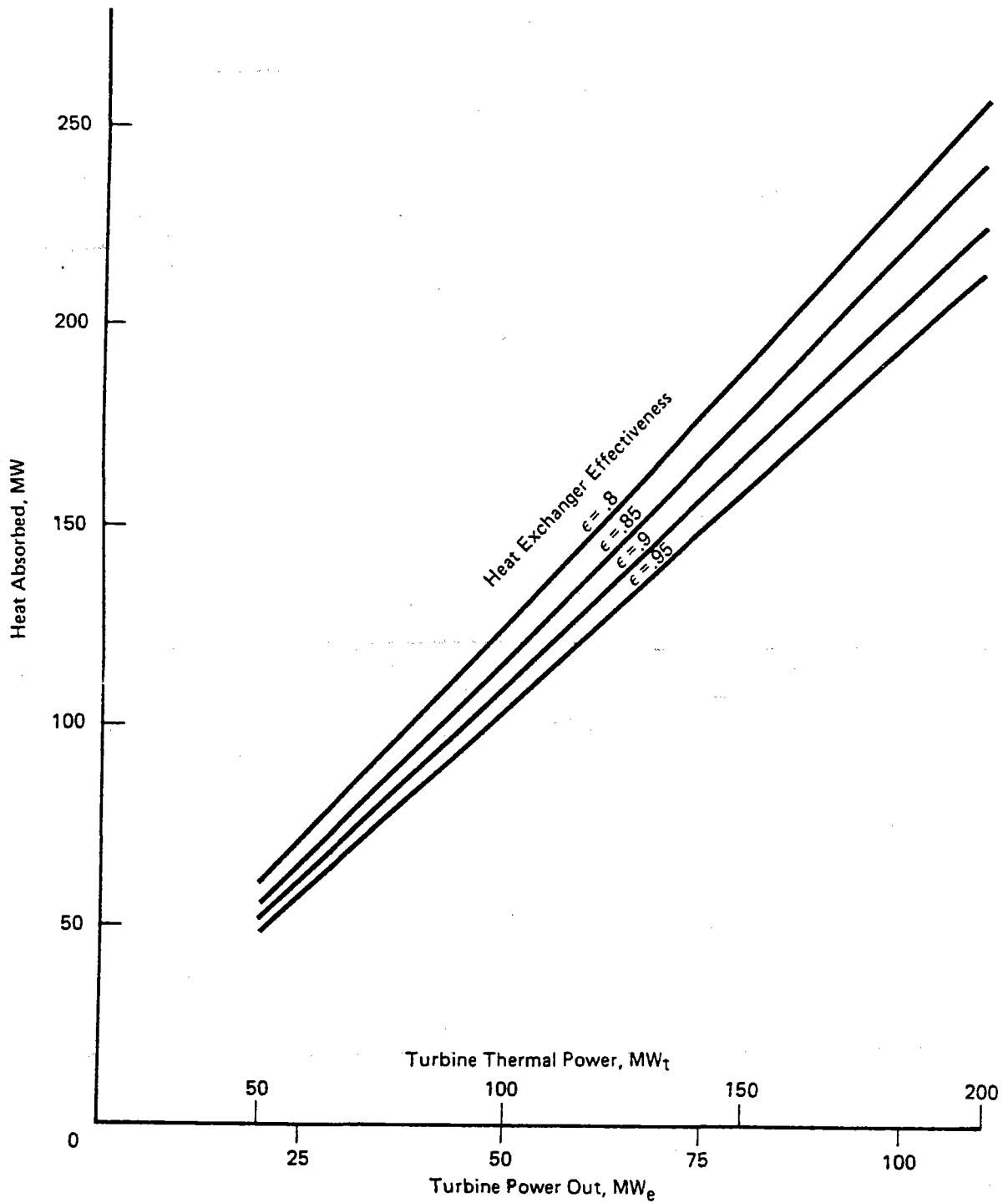


Figure 3 PIR-ISTIG Thermal Requirements as a Function of Load

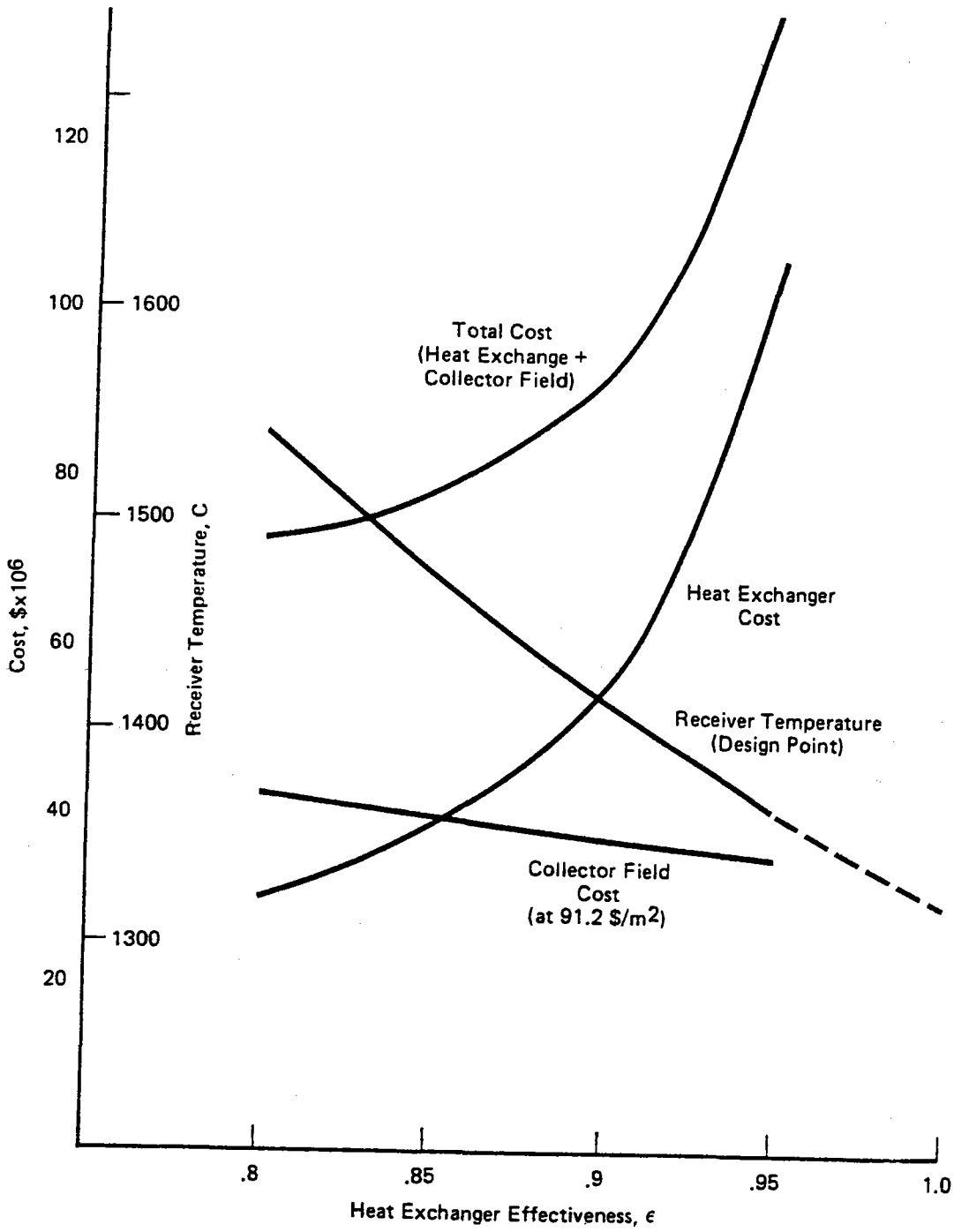


Figure 4 Heat Exchanger and Heliostat Cost Trade-off as a Function of Heat Exchanger Effectiveness

considered feasible to achieve in this application was 1480°C , a heat exchanger effectiveness of 0.85 was selected.

A reduction in the heat exchanger cost to about 1/3 of that shown is required to move the optimum to a higher heat exchanger effectiveness. The result is a lowering of the receiver temperature, a reduction in the receiver absorbed power and a lowering in the system costs. The impact of such an improvement in the cost of ceramic heat exchangers is discussed in Section 5.

4.0 PIR SYSTEM DESIGN

For the purpose of this study, only those portions of the solar central receiver power plant particular to the particle injection receiver were designed. These consist of the collector field, the thermal regions of the receiver (aperture and heat absorption region), the heat exchanger, the ducting and exhaust fan and the particle injection system.

4.1 Collector Field

The collector field was designed to give the least cost combination of heliostats, receiver aperture, and tower, while maintaining fluxes in the receiver aperture which were suitable for particle heating. DELSOL3 was used to analyze the collector field and to perform the optimization.

The results of the DELSOL3 optimizations are given in Table 1. In all the cases shown, a 2-D smart aiming strategy was used to give a flux distribution fairly uniform across the aperture, but concentrated toward the bottom. For the small glass-metal heliostats, the 18 m wide x 16 m high aperture gave the best field efficiency and still had a peak flux greater than 2.5 MW/m^2 . This collector field, tower and aperture were selected because the required receiver temperatures could be reached with minimum particle mass loading under these conditions. Once the receiver aperture size was selected and the receiver flux distribution calculated, the receiver flow parameters were established and the receiver suspension parameters determined to maximize the receiver outlet temperature.

Table 1
COLLECTOR SYSTEM DESIGN SUMMARY

Aperture Width (W) and Height (H)	Heliostat Type			
	58.5m ² Rectangular Glass/Metal			150m ² Stressed Membrane
	16W x 14H	16W x 16H	18W x 16H	18W x 16H
1. Tower Height (m)	200	200	190	195
2. Number of Heliostats	8446	8246	8219	3027
3. Mirror (m ²) Area	494300	482560	481000	454100
4. Land (km ²) Area	2.44	2.30	2.33	3.14
5. Field Efficiency	.470	.486	.496	.554
a) Heliostat Reflty	.920	.920	.920	.920
b) Cosine	.839	.84	.837	.835
c) Shad&Block	.930	.929	.931	.963
d) Atm. Trans.	.929	.93	.931	.922
e) Intercept	.820	.852	.875	.956
f) Receiver	.860	.855	.850	.850
g) Piping	1	1	1	1
6. Peak Flux (MW/m ²)	3.37	3.14	2.86	3.21

As input to a sensitivity analysis, a collector field was also designed for the 18m wide x 16m high aperture using 150 m² stressed-membrane heliostats. Because it was assumed that these heliostats give a better-defined beam, there is less spillage at the receiver and less mirror area in the collector field. In addition, the receiver flux is higher and more evenly distributed across the aperture. Results of these calculations are discussed in the next subsection.

4.2 Receiver Heat Absorption Region Design

The heat absorption region consists of particle-laden flow traveling upward through the receiver, normal to the solar flux. The particles heat by absorption as they pass through the solar flux, heating the adjacent air by conduction. As the particles reach temperatures above about 1300K they begin to oxidize, burning up with time and increasing temperature. As the particles burn and decrease in size, they permit the solar flux to penetrate deeper into the particle suspension.

To match the solar flux distribution, which decreases away from the centerline, the back wall of the receiver is shaped in a smooth curve to give a thicker flow stream in the center and thinner flow stream on the edges. Once the aperture dimensions, flow rate, and velocity are selected, the receiver flow thickness and flux intensity are properly balanced so that all particles throughout the receiver heat and oxidize by the time they reach the top of the aperture, giving air which is heated, but free of carbon particulates.

For the 110 MWe ISTIG cycle, the design receiver flowrate is 161 kg/s, which allows a 10% "curtain" flow which is used to minimize disturbance to the particle-laden flow. The flow velocity is 40 m/s and the particle generation rate was selected to give 1.0 gm of carbon/m³ of air. A particle diameter of 0.3 microns was selected to give optimum performance in the receiver. The oxidation rate for these particles is:

$$k(\text{g/cm}^2\text{-s-atm}) = 257 \exp(-21460/T(\text{K}))$$

These parameters were selected on the basis of previous optimization studies (reported in Ref. 3) and through additional calculations using the computer model 2DPRTS, which computes temperature rise, particle oxidation, and energy balance as a function of time and location throughout the receiver for a given flux distribution. This 2DPRTS calculation is done by subdividing the flow into 2 dimensional control volumes. For a vertical cross section through the depth of the flow, small steps are taken in the flow (X) direction for finite streamlines in the depth (Y) direction. The optimization was also used to maximize temperature uniformity across the aperture by computing temperatures at the centerline and near the edge and then adjusting the flow thickness, by adjusting the shape of the wall. Temperatures were then weighted across the aperture to calculate bulk temperature. The input and results for the four selected power levels are listed in Table 2.

Table 2

RECEIVER HEAT ABSORPTION REGION
DESIGN PARAMETERS

Turbine Output, MWe	Receiver Absorbed Power, MWt	Receiver Mass flowrate (air + steam), kg/sec	Particle Mass Loading, g/m ³	Final Temperature, °K	Losses %
110	242	161	1.0	1752	15
81.6	180	132	1.1	1655	14.5
50.4	118	96	1.2	1548	14.0
19.3	57	51	1.4	1443	13.5

Velocity = 40 m/s

Particle diameter = 0.3 microns

As indicated, the design point conditions were achieved using a particle mass loading of 1.0 gm/m³. At lower loads, the temperatures were reached by increasing the mass loading to increase the effective absorption of the medium. In practice, this would be accomplished by adjusting the particle generation rate relative to air mass flowrate.

As mentioned previously, flux maps were also calculated for the case of 150m² stressed-membrane heliostats. Using the flux map generated for these heliostats, and the design point aperture and receiver flow conditions, a 15% higher temperature rise was achieved. These calculations show two advantages: 1) while using less collector field area, higher temperatures can be achieved in the receiver, and 2) these higher temperatures can be used to either reduce heat exchanger effectiveness (less capital cost) or reduce particle mass loading (less operating cost). The significant improvement achieved with the stressed-membrane heliostats is due to the significantly better beam quality that were assumed compared to those for the 2nd generation glass-metal heliostats.

4.3 Receiver Aperture and Backwall

Solar insolation is reflected off the heliostats and focused on the receiver aperture. The average angle of reflection for the solar insolation incident on the receiver is 22.5°. Thus, the aperture and receiver cavity back wall are inclined at an angle of 22.5° with the vertical. This ensures that the major portion of the particle laden air stream passes normal to the concentrated solar flux for maximum heat recovery. The back wall is insulated using ceramic Pyro-Bloc insulation that has been rigidized with a liquid rigidizer to prevent erosion of the surface.

The receiver air streams (particle-laden and air curtain) travel at a uniform velocity through the receiver cavity. A skimmer attached to the upper lip of the receiver aperture is used in conjunction with the air curtain flow control vanes to direct the flow of the high temperature gas stream into the inlet plenum of the high temperature ceramic heat exchanger.

In order to minimize thermal cycling of the ceramic heat exchanger and to avoid start-up delays associated with warming the heat exchanger, the receiver is equipped with sliding doors that are closed at night and during extended outage. The external surface of the doors and the north

face of the receiver are insulated with high temperature ceramic insulation.

4.4 High Temperature Ceramic Heat Exchanger

The air-to-air heat exchanger in the PIR-ISTIG concept consists of a high temperature ceramic portion followed by a lower temperature metal portion. Hot air from the heat absorption region of the receiver is ducted into the high temperature ceramic heat exchanger. The heat exchanger is fabricated using reaction-bonded silicon carbide tubes. A bayonet-type tube configuration is used to reduce thermal stresses due to external temperature excursions. The bayonet elements are arranged vertically in two rows with their ends along the centerline and their headers at the top and bottom of the module assembly. The ceramic tubes have smooth walls. The slight improvement in heat transfer performance obtained using finned ceramic tubes does not warrant their use. Finned ceramic tubes are substantially more expensive and historically problem prone. The length of the tubes is limited to 3.05 m (10 ft) by the current size of commercial ceramic furnaces. The tubes are manifolded together by the heat exchanger fabricator to form bays or modules. The modules are then connected in situ to form the assembled unit.

At the design point, the temperature of the hot receiver air exiting the ceramic heat exchanger is about 871°C . This design temperature was selected on the basis of the upper temperature limit for the metallic heat exchanger. The design inlet temperature for the ceramic heat exchanger is 1480°C . At the design point, pressurized air enters the tube side of the ceramic heat exchanger at about 700°C and exits at 1328°C .

At the high temperatures employed in this heat exchanger, radiation exchange between the tubes must be considered. As the tube spacing increases:

- The mean beam length for radiation increases and the radiation heat transfer increases

- The velocity of air past the tube decreases and the convective heat transfer drops
- The duct side pressure drop decreases and the fan power decreases

The heat exchanger was designed with an allowable duct side pressure drop of 40 cm (15.75 in.) of water and a tube side pressure drop of approximately 60 kPa. The allowable duct side pressure drop lead to a relatively wide tube spacing of about 15.24 cm (6 in.). Fortunately, the radiative interchange between the tubes counteracted the reduced convective heat transfer to produce an acceptable design.

4.5 Metallic Heat Exchanger

After the hot receiver air passes through the ceramic heat exchanger, the remaining heat is extracted from the stream in a metallic finned-tube heat exchanger. To keep the headering requirements to a minimum, 9.1 m (30 ft) tubes are used. Thermal stressing of the heat exchanger elements is kept to a minimum by mounting the tubes vertically and fixing the header at one end while allowing the other end to float. The tubes are grouped into modules, and these modules are manifolded together.

The allowable pressure drop on the duct side of the heat exchanger is approximately 5 cm (1.97 in.) of water, and the tube pressure drop is 7 kPa. At the design point, the inlet temperature of the duct side air is 871°C and the exit temperature is 574°C. This available heat is sufficient to raise the air temperature on the tube side from 400°C to 700°C. The heat exchanger insulation and support is similar to that for the high temperature ceramic heat exchanger.

A transitional duct connects the duct side exit of the high temperature ceramic heat exchanger to the inlet of the metallic heat exchanger.

4.6 Ducting and Fans

Air heated in the solar receiver exits at a maximum temperature of about 1480°C. The receiver surfaces in contact with these hot gases are

insulated with ceramic insulation. The ceramic insulation selected for the receiver cavity and the ducting between the receiver and the heat exchangers is a flexible, modular type insulation similar to the Pyro-Bloc Y modules manufactured by Babcock & Wilcox. The insulation modules are approximately 0.3 m by 0.3 m by 0.3 m (12 in. by 12 in. by 12 in.). During installation, the modules are compressed against adjacent modules. This ensures that the seams between modules do not open during daily cyclic operation of the receiver. Any continuous break in the insulation could result in substantial decrease in thermal performance and structural damage to the receiver. Ceramic Pyro-Bloc insulation - with a density of 190 kg/m^3 (12 lb/ft^3) and thickness of 30.48 cm (12 in.) - is sufficient to maintain the cold face temperature at less than 80°C when the hot face temperature is 1300°C .

The flow of the hot air from the receiver is induced through the duct side of the heat exchangers using an induced draft centrifugal fan. Other options, including natural-draft induced flow using a chimney and compressed air operated educators, were previously evaluated and found to be inferior to the induced draft fan.

At the design heat exchanger flow rate of 161 kg/s (354 lb/s), the centrifugal fan will generate a suction equivalent to 50 (13 in.) of water and will consume about 1.25 MWe.

A much smaller centrifugal fan is used to generate air for the receiver auxiliary air flow. The blower exhaust is ducted directly into the receiver area. The direction and thickness of the auxiliary airflow are controlled by damping vanes attached to the end of the duct. The centrifugal fan for the air curtain consumes 50 kWe.

4.7 Particle Generator

The basis for the present design of the particle generation system is the furnace process, which is used in the production of carbon black. Although either oil or natural gas could be used as feedstock for the particle generation, oil is the selected feedstock, because solar

generation facilities are usually located at remote sites where natural gas is generally not available. In addition, oil has a higher carbon-to-hydrogen ratio and can provide a higher carbon yield. Among the various oil grades available, gas oil with high aromatic content is preferred because it has the highest carbon yield. For this system, gas oil with an HHV of 17,700 Btu/lb was assumed.

The particle generation system consists of a reactor, oil storage tank, oil pumps, and oil preheater. The oil storage tank and pumps would be placed at ground level; the reactors and oil preheaters would be placed on the top of the solar tower.

The reactor is a double shell, refractory lined, horizontal cylindrical vessel. It consists of a combustion zone and a reaction zone. The particle size is a function of the reaction temperature and residence time. In general, a lower reaction temperature and a longer residence time favors a larger particle size. The particle size required for the particle injection receiver is in the coarse particle size range of the carbon black produced commercially.

The particle generation system has been designed for atmospheric pressure operation. Pressurized operation was not selected because the control valve required to regulate the pressure is not commercially available for high reactor exhaust temperature. To increase turndown capability and increase reliability, two 50 percent capacity units were selected.

Twenty days of oil storage was assumed. The tank is a vertical cylindrical API tank with the necessary diking to prevent spillage. One tank with no spare is used.

The oil pump delivers oil from the oil storage tank at grade to the oil preheater on the solar tower. This oil pump requires a low flow high head pump. Two multistage centrifugal pumps (one operating and one spare) were selected to ensure high reliability.

The oil preheater consists of a flat finned-tube bundle placed in the exhaust air stream coming from the heat exchangers. The heat in the exhaust air preheats the oil to 200°C to facilitate oil vaporization in the reactor.

The major operating parameters that must be controlled are residence time and reaction temperature. The residence time is controlled by regulating the air flow. The reaction temperature is controlled by regulating the air-to-oil ratio.

4.8 Particle Injection/Distribution

Carbon particles that are generated in the particle generators are ducted to the turbine exhaust through high temperature ducts. The particle-laden streams from the generators are allowed to mix before they enter the turbine exhaust region. Ceramic screens in the ducts promote mixing and ensure an even distribution of particles in the turbine exhaust ducts. A guillotine type shut off is provided to isolate each of the particle generators in the event that one should fail. This will allow the system to run at partial load.

The major portion of the turbine exhaust flow (90 percent) is used to quench the particles and carry them into the receiver area. The remaining (10 percent) turbine exhaust flow is ducted to the receiver area through separate nozzles and is injected as part of the "curtain" air stream parallel to the particle stream.

5.0 PERFORMANCE AND COST

5.1 Receiver Efficiency

The particle injection receiver is extremely energy efficient compared with previous air heating solar receiver concepts. Less than 15% of the energy incident on the aperture is lost to the environment through scattering and thermal emission. Of this amount, about 90% is lost by scattering from the particles; the other 10% is lost by thermal emission. The reason for this performance lies in the physics of the interaction of solar radiation with the small particles. Particle

scattering processes have been studied in general and are described in Reference 4. The potential for solar application was first explored by Hunt, whose work is described in References 5-7. The key factors in the efficient heat exchange which occurs in the PIR can be summarized as follows:

- Small particles (≤ 1 micron diameter) are very good absorbers of solar radiation because the particles are about the same size as the wavelength of the solar radiation. This is especially true for carbon particles because carbon has a high intrinsic absorptivity.
- The back scattering cross section is approximately an order of magnitude less than the absorption cross section.
- The thermal emission rate is orders of magnitude smaller than the absorption rate over most of the spectral and temperature range. The emission rate is appreciable only for temperatures immediately preceding particle burnout, i.e., the particles oxidize and disappear within milliseconds, at the same time as they begin to radiate appreciably.

Figure 5 illustrates the relative strengths of the absorption, scattering and radiation processes in the front layer. Figure 5 also shows the temperature rise and particle oxidation (decrease in radius) as a function of distance (time). The competition between radiation and oxidation effects is clearly seen in the radiation flux curve as it increases with temperature and then decreases with decreasing particle size. The curve labeled "Blackbody Radiator" shows the energy loss which the particles would experience if they were blackbody radiators. The difference between the "Blackbody" curve and the emitted flux is due to the real optical properties of carbon. In fact, the properties of carbon make it ideal for this application because absorption is good over the visible solar spectrum and suppressed in the infrared. These properties are illustrated in Figure 6, which is adapted from Ref. 8.

In Figure 7, an envelope has been sketched to enclose the absorption, scattering and radiation curves for all the discrete layers in the flow field, which were modeled in the computer calculation. The curves for

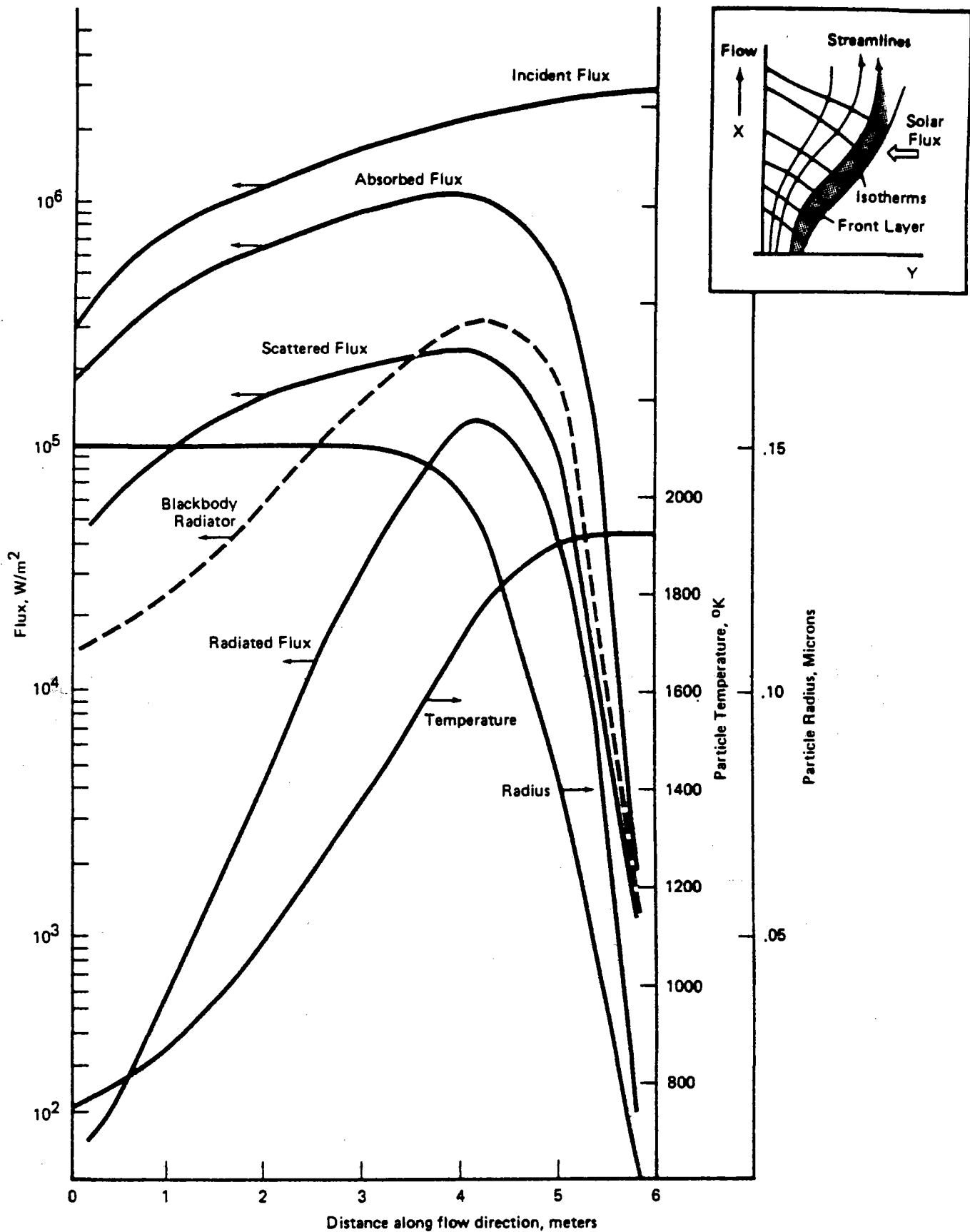


Figure 5 Calculated Fluxes, Particle Temperature and Size for the Front Layer of the Design Case

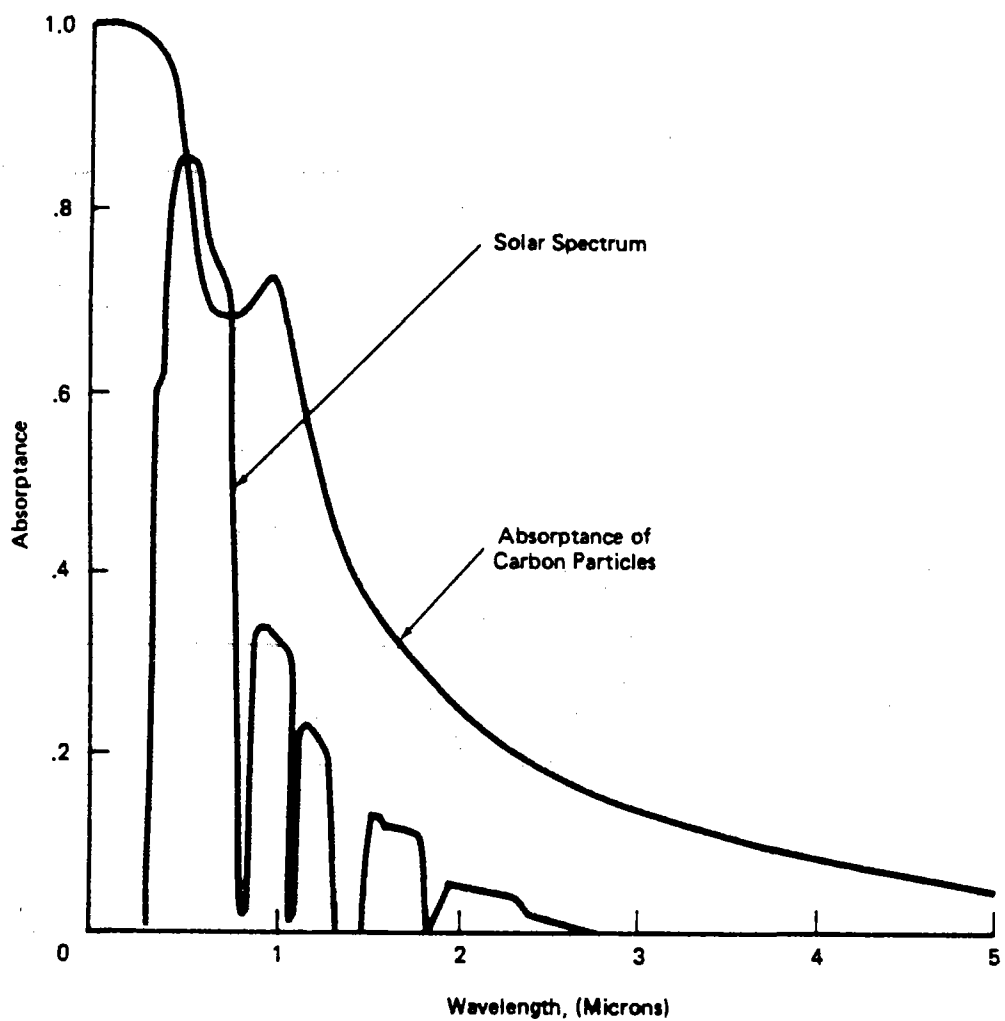


Figure 6 Wavelength Dependence of the Absorbance of a Carbon Particle

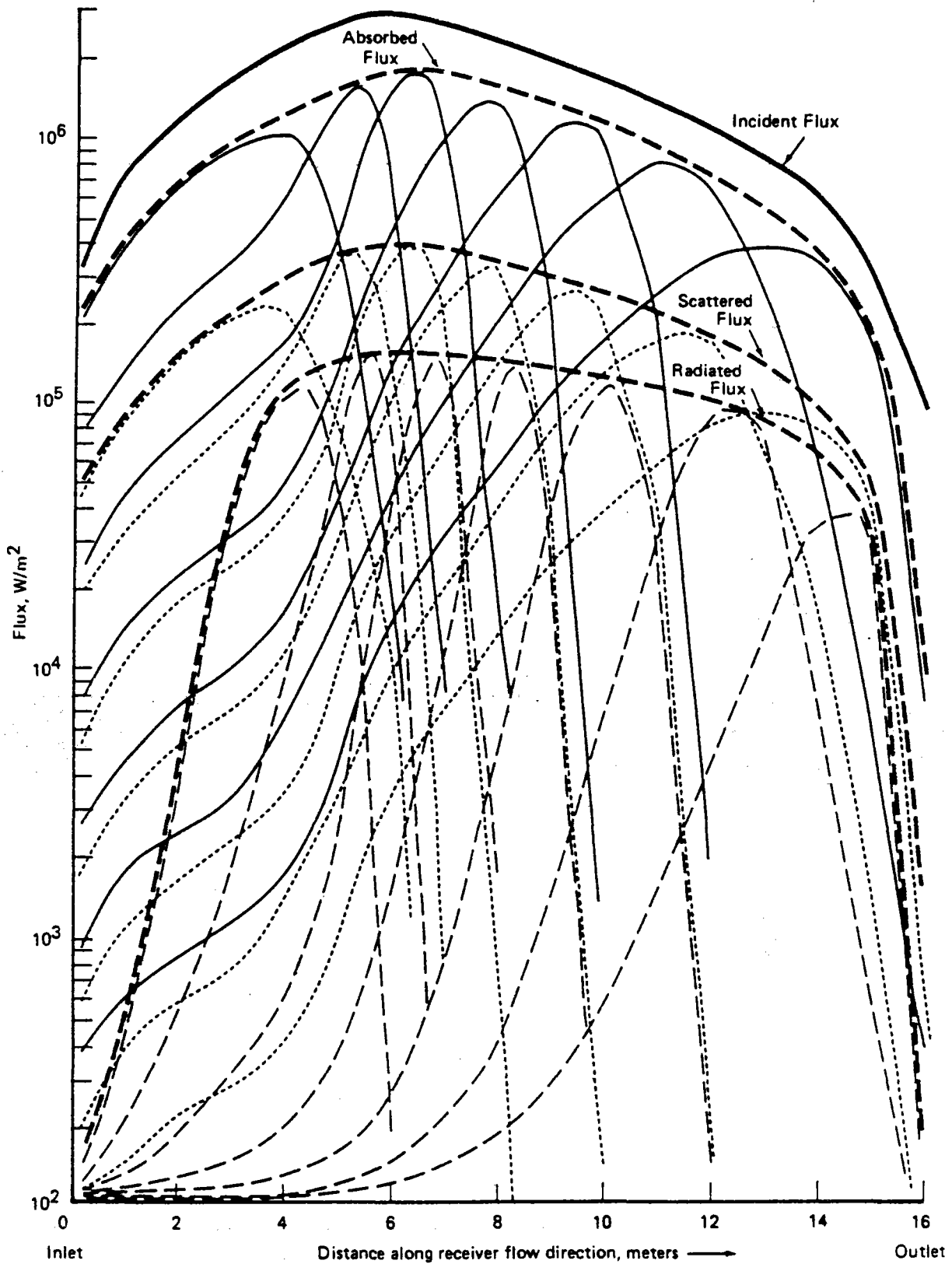


Figure 7 Calculated Fluxes for all Flow Streams Along the Flow Direction (Design Case, Centerline)

individual stream layers show that absorption takes place mostly in the front-most layer until the particles heat and begin to oxidize. Then, as the solar flux penetrates deeper into the flow, deeper layers begin first to absorb and then radiate. Scattering and absorption intensities increase together in a given layer, but radiation lags until the temperature becomes significant. Then all three processes decrease rapidly as the particles shrink. A real flow would not be divided into discrete layers; rather, the absorption and heating processes would move gradually deeper into the particle-laden flow as it flows through the solar flux. The envelopes indicate the overall relative strengths of the absorption, scattering and radiative processes.

A 90% receiver efficiency had been calculated for the PIR-Brayton cycle, as reported in Ref. 3. The receiver efficiency of 85% for the PIR-ISTIG cycle is somewhat lower because of:

- higher scattering losses due to the larger particles which were needed to reach the higher temperatures of this cycle
- higher radiative emission losses, also due to the higher temperatures.

In addition to these differences, the ISTIG cycle injects about 13% water vapor into the receiver working fluid. This water vapor will also absorb and radiate energy over the solar spectral region, primarily due to vibration excitation of the H_2O molecule. Air, on the other hand, does not absorb or emit radiation because O_2 and N_2 molecules are symmetric.

The processes of absorption and radiation by water vapor in the air are not included in the 2DPRTS model. However, hand calculations using the blackbody emittance (ranging from about 0.08 to 0.15 over the PIR temperature range) and Beer's law to approximate optical depth indicate that both absorption and losses per unit volume of air will be about 10% higher. The impact of this effect could be to speed up the heating processes, so that a smaller aperture is required. Because of multiple competing processes (absorption, conduction, backscatter, radiation and

oxidation all as a function of depth and time), it is difficult to quantitatively estimate the effect without a detailed model.

5.2 Impact of Direct-Contact Heat Exchanger

If the shell and tube ceramic/metal heat exchanger were replaced with a direct-contact heat exchanger, the energy input and temperatures required in the receiver would be reduced. This reduces the collector field requirements and, to a small degree, reduces the thermal losses from the receiver. A reduction in the particle mass loading and a smaller aperture size may also be possible for such a system. For example, if a heat exchanger effectiveness of 1.0 could be achieved, then only 200 MWt and a maximum receiver temperature of 1320°C would be required. This represents a 17% reduction in collector field requirements to produce the incident flux. Also, since this temperature is approximately that which was the basis for the Bechtel-funded feasibility study (Ref. 1), it is possible to roughly estimate a 20% reduction in particle mass flowrate and a combined scattering and radiation loss of only 10%. A detailed calculation would be required to give more accurate estimates of all the reductions possible under the conditions resulting from the use of a direct-contact heat exchanger.

5.3 PIR System Costs

The cost of the solar-related components of the PIR system are listed in Table 3. In addition to the collector field, receiver, and heat exchanger, are the particle generator, exhaust fan and auxiliary blower. A fuel flowrate of 12.3 lb/hr at full load is also required. Fuel costs can be estimated at approximately \$20/bbl.

6.0 CONCLUSIONS

The above analyses show that the particle injection receiver can be used to effectively drive an ISTIG power cycle. The receiver appears capable of achieving the required outlet temperatures at an efficiency of 85% with no degradation in performance at part load conditions. Both the receiver efficiency and the receiver intercept are improved when using 150m² stressed-membrane heliostats with a reflected beam error standard

Table 3

PIR SYSTEM COMPONENT INSTALLED COSTS

	Weight (Tons)	Factory Equipment (\$1000)	Site Labor (Hrs)	Labor Rate (\$/Hr)	Site Labor (\$1000)	Site Material (\$1000)	Total Cost (\$1000)
1. Ceramic HX	1474	35,600	8,000	45	360	36	36,000
2. Metal HX	220	2,500	1,333	45	60	5	2,565
3. EXH & Motor	70	240	688	45	31	6	280
4. Part. Gen.		202	1,460	50	73	116	390
5. Blower-Curtain		170	790	45	36	7	210
6. Rec. Structure		0	22,285	35	780	1,055	1,835
							41,280

deviation of 1.7 milliradians compared to the 58.5m² 2nd generation glass-metal heliostats with a reflected beam error of 5.2 milliradians. For the assumed installed collector field cost of 91.2 \$/m², the ceramic heat exchanger is the major cost component in the plant. The ceramic heat exchanger cost estimate is based upon today's materials technology and manufacturing techniques. It is generally expected that ceramic heat exchanger technology will improve and costs will come down in the future. A heat exchanger cost reduction to about 1/3 of the current cost would result in the selection of a 90% effective ceramic heat exchanger and reduce the total PIR component cost estimate (including collector field cost) by \$22M.

Specific areas of experimental research necessary for developing a better understanding of the particle injection receiver concept are summarized below. A complete development plan would consist of analysis and laboratory-scale experiments, engineering design studies, and subsystem and system experiments. The most important near-term elements of that development plan are:

- **Particle oxidation rate data.** A variety of particles and particle generation techniques should be explored and testing should be undertaken with actual concentrated sunlight. Precise oxidation rate data are need for these particles as a function of particle size, temperature, and solar flux intensity.
- **Receiver fluid mechanics.** The fluid mechanical model of the behavior of the darkened air stream needs to be verified through combination of more detailed analytical techniques and small-scale experiments.
- **Particle optical properties.** The wavelength-dependent complex index of refraction is used to calculate absorption and scattering efficiencies. The values used in this study were derived from measurements on carbon films at ambient temperature. Although these data are adequate for the purpose of the present study, data on actual particles at real receiver temperatures are desirable. These measurements can be performed systematically in a laboratory under controlled spectral and thermal conditions.

Specific elements of a particle injection receiver development plan relating to the ISTIG application are:

- Inclusion of water vapor in thermal model. Both the absorption and the emission of water molecules must be included in the receiver heat absorption model to correctly determine the impact on the heating rate, the aperture size, the thermal emissions, and the achievable outlet temperature.
- System optimization studies. Further investigation of the optimal characteristics of a PIR-ISTIG power plant is warranted in the areas of:
 - Investigate alternative heat exchange configurations, including a direct contact heat exchanger and a ceramic thermal storage system cycling between unpressurized (charging) and pressurized (discharging) operation.
 - Investigate the value of thermal storage vs. fossil hybridization.

REFERENCES

1. "Feasibility Study of a High Temperature Solar Central Receiver Gas-Turbine Power Plant," Report on a Bechtel Technical Grant, Bechtel National Inc., March 1987.
2. "Scoping Study: LM5000 Steam-Injected Gas Turbine," Report No. 84-STIG-1, Prepared for Pacific Gas and Electric Company by General Electric Company, 1984.
3. Schoenung, S. M., De Laquil III, P., and Loyd, R. J., "Particle Suspension Heat Transfer in a Solar Central Receiver," Proc. of the ASME/JSME Joint Solar Engineering Conf., Honolulu, Hawaii, March 1987.
4. Bohren, C. F. and D. R. Huffmann, Absorption and Scattering of Light by Small Particles, Wiley, New York, 1983.
5. Hunt, A. J., "Small Particles Heat Exchangers," Lawrence Berkeley Laboratory Report 7841, 1978.
6. Hunt, A. J. and C. T. Brown, "Solar Test Results of an Advanced direct Absorption High Temperature Gas Receiver," Proceedings of the 1983 Solar World Congress, Perth, Australia, August 1983.
7. Yuen, W. W., F. J. Miller, and A. J. Hunt, "Heat Transfer Characteristics of a Gas-Particle Mixture Under Direct Radiant Heating," Intl. J. Heat and Mass Trans, 1984.
8. Hunt, A. J., "Optical Properties of Small Particle Suspensions for Solar Thermal Collection," Lawrence Berkeley Laboratory Report 10221, 1980.

SERI 

APPENDIX B
Major Technical Uncertainties

Appendix B Major Technical Uncertainties

Table B-1 lists the major areas of technical uncertainty associated with the ISTIG engine and each of the receiver types. The table also lists (necessarily somewhat subjective) assessments of that technological area. The first assessment indicates the importance of that area to the success of the system. If the area is critical to the viability, then the importance will be major; but if there are several likely alternatives, the importance will be minor. The second assessment indicates the risk of resolving the uncertainty favorably. If the uncertainty requires major quantum leaps forward in technology, then the risk would be high. On the other hand, if the required advances are reasonably small and in a direct line from current work in the area then the risk would be low.

Although all of the systems examined here have important technological areas in which research and development is needed, they will not all require the same amount of research and development effort. However, it was beyond the scope of this study to attempt to accurately estimate either the funding levels required or the probability of success for the competing technologies. The reader can, however, use the data given here as a starting point for such an assessment.

Most of the uncertainties associated with the ISTIG engine are either fairly minor or will probably be resolved outside of the Solar Thermal Technology Program. As mentioned above, it seems likely that advances in stationary gas-turbine efficiency will proceed independently of solar applications. The "solarizing" (developing an externally-fired version) of the particular engine chosen here is listed as medium risk because there may not be any incentive for the manufacturer to make this investment. The fact that the engine is expected to be in development by 1988 caused this item to be labeled low risk.

The single most significant uncertainty for the high-temperature DAR is the working fluid. It is of major importance to the success of the system and, when identified, may well present any number of design challenges (much as the carbonate salts for 900°C applications did [B-1]).

Although the mechanisms that the PIR concept relies on are well understood and documented, the carbon particle reaction rates and the bulk heat transfer characteristics of the particle cloud require better definition. The needed parameters have largely been bounded, but better numbers are necessary for detailed design work. Controlling the flow of expanding air across this large (18 m by 16 m) aperture may be a significant challenge. However, the relatively high velocities (40 m/s) and the coincidence of the forced flow with the bouyant forces should be helpful here.

The challenges associated with the heat exchangers apply to both the PIR and the volumetric receiver. The fundamental issue here is overcoming the poor heat-transfer characteristics of the low-pressure air. The ceramic AAHX is largely a known, commercially available entity for pressures up to about 10 atm (the ISTIG engine uses 30 atm). However, the cost is currently high, which leads to fairly low heat exchanger effectiveness and high receiver temperatures. A factor of 3 reduction in cost would be required to increase the optimum heat exchanger effectiveness to 0.90 (see Section 3.0 in Appendix A). By contrast, although a working fluid for the DCHX has not been identified, the estimated cost and performance offer substantial gains over the AAHX.

Table B-1. Major Technical Uncertainties

Area of Uncertainty	Importance/Risk
<u>ISTIG</u>	
Tower-top location	minor/low
Operation and maintenance costs relative to steam/Rankine	minor/low
Solar-fired without significant loss of efficiency	minor/medium
Not commercially available today	major/low
<u>High-Temperature DAR</u>	
Identification/selection of a high-temperature working fluid	major/medium
corrosion	
containment	
pumping	
contact with moist air	
optical dopants	
<u>PIR</u>	
Particle characteristics	major/low
oxidation rates	
size distribution	
bulk radiative properties	
Fluid dynamics	major/medium
control of high-temperature, high-speed flows over a large area	
control of particle distribution	
<u>Volumetric Receiver</u>	
Fiber service characteristics	major/medium
flux capabilities	
strength	
life	
Air flow distribution	major/medium
Radiative/convective heat-transfer modeling	major/low
<u>Heat Exchangers</u>	
Ceramic AAHX at high pressure	major/low
DCHX working fluid (containment, pumping, compatibility with hot air/steam mixture, etc.)	major/medium

The most commonly mentioned candidate for fibers in the volumetric receiver is silicon carbide. However, use of these fibers in very small diameters under high flux levels has not been demonstrated and will probably create some design challenges, leading to classification of this area as major importance and medium risk. Much of the experimental work that has been done on the volumetric receiver to date has been without the benefit of a good generalized analysis of the heat transfer within the fiber pack*. This analysis is needed before any further work is done on the concept. Finally, the heat exchanger issues faced by the volumetric receiver are identical to those facing the PIR, with the exception that the high losses associated with the AAHX hurt the volumetric receiver performance even more than the PIR.

References

- B-1 Coyle, R. T., T. M. Thomas, and P. Schissel, The Corrosion of Materials in Molten Alkali Carbonate Salt at 900°C, SERI/TR-255-2553, Golden, CO: Solar Energy Research Institute, June 1985.
- B-2 Schoenung, S. M., P. DeLaquil III, and R. J. Loyd, "Particle Suspension Heat Transfer in a Solar Central Receiver," Solar Engineering - 1987, Proceedings of the 1987 ASME Solar Division Conference, March 1987.
- B-3 Skocypec, R. D., Boehm, R. F., and Chavez, J. M., "Heat Transfer Modeling of the IEA Volumetric Receiver," presented at the AIChE 23rd National Heat Transfer Conference, 1988.

*Drost at Pacific Northwest Laboratory analyzed several cases fairly carefully [B-2] but for a very limited range of parameters (e.g., a single geometry, uniform fluxes, and a single fiber diameter). More recently, Skocypec, Boehm, and Chavez [B-3] have developed a two-flux model of the fiber pack but have not exercised it extensively.

SELECTED DISTRIBUTION LIST

ARCO Solar, Inc.
9315 Deering
Chatsworth, CA 91311
Jim Caldwell

Acurex Solar Corporation
485 Clyde Ave.
Mt. View, CA 94042
Don Duffy

Advanco Corporation
40701 Monterey Ave.
Palm Desert, CA 92260
Byron Washom

Arizona Public Service Company
P.O. Box 21666
Phoenix, AZ 85036
Eric Weber

BDM Corporation
1801 Randolph SE
Albuquerque, NM 87106
J. Alcone

Babcock and Wilcox
91 Stirling Ave.
Barberton, OH 44203
Paul Elsbree

Barber-Nichols Engineering Co.
6325 W. 55th Ave.
Arvada, CO 80002
Robert Barber

Battelle Pacific NW Laboratory
P.O. Box 999
Richland, WA 99352
Kevin Drost
Tom A. Williams

Bechtel Corporation
P.O. Box 3965
San Francisco, CA 94119
Pascal DeLaquil

Black and Veatch Consulting Engineers
1500 Meadow Lake Parkway
Kansas City, MO 64114
John Harder

Tom Brumleve
Consultant
1512 N. Gate Road
Walnut Creek, CA 94598

Tibor Buna
32689 Inverness Dr.
Evergreen, CO 80439

Department of Energy/HQ
Forrestal Building
1000 Independence Ave., SW
Washington, DC 20585
H. Coleman
S. Gronich
C. Mangold
M. Scheve
Frank Wilkins

Department of Energy/SAN
1333 Broadway
Oakland, CA 94536
Robert Hughey
William Lambert

Department of Energy/SAO
1617 Cole Blvd.
Golden, CO 80401
Paul Kearns

Electric Power Research Institute
P.O. Box 10412
Palo Alto, CA 94303
Donald Augenstein

Christopher England
Consultant
Engineering Research Group
138 West Pomona Ave.
Morrovia, CA 91016

Entech, Incorporated
P.O. Box 612246
DFW Airport, TX 75261
Walter Hesse

Foster Wheeler Solar Development Corp.
12 Peach Tree Hill Road
Livingston, NJ 07070
S. F. Wu

Gas Research Institute
8600 West Bryn Mawr Ave.
Chicago, IL 60631
Keith Davidson

Georgia Tech Research Institute
Energy and Materials Sciences
Laboratory
Atlanta, GA 30332
Tom Brown

LaJet Energy Company
P.O. Box 3599
Abilene, TX 79604
Monte McGlaum

Lawrence Berkeley Laboratory
Building 90-2024,
University of California
1 Cyclotron Road
Berkeley, CA 94720
Arlon Hunt

Luz Engineering Corp.
15720 Ventura Blvd.
Suite 504
Encino, CA 91436
David Kearney

Martin Marietta
P.O. Box 179
Denver, CO 80201
Tom Tracey

Mechanical Technology, Inc.
968 Albany Shaker Road
Latham, NY 12110
H. M. Leibowitz
G. R. Dochat

Midwest Research Institute
425 Volker Blvd.
Kansas City, MO 64110
R. L. Martin
Jim Williamson

NASA Lewis Research Center
21000 Brookpark Road
Cleveland, OH 44135
Dennis Flood

Power Kinetics, Inc.
1223 Peoples Ave.
Troy, NY 12180
Bob Rogers

Sanders Associates, Inc.
95 Canal Street
Nashua, NH 03010
Daniel J. Shine

Sandia National Laboratories
Solar Energy Department 6220
P.O. Box 5800
Albuquerque, NM 87185
John Otts
James Leonard
Donald Schuler
Craig Tyner
Russ Skocypec

Solar Energy Industries Association
1717 Massachusetts Ave. NW No. 503
Washington, DC 20036
Carlo La Porta
David Goren
Hal Seilstad

Solar Energy Research Institute
1617 Cole Blvd.
Golden, CO 80401
B. P. Gupta
Gerold Groff

Solar Kinetics, Inc.
P.O. Box 47045
Dallas, TX 75247
Gus Hutchison

University of Houston
4800 Calhoun
106 SPA Building
Houston, TX 77004
Lorin Vant Hull

Document Control Page	1. SERI Report No. SERI/TR-253-3196	2. NTIS Accession No.	3. Recipient's Accession No.
4. Title and Subtitle High-Temperature Solar Central Receivers for Electricity Production		5. Publication Date June 1988	
7. Author(s) J.V. Anderson, N. Weaver		8. Performing Organization Rept. No. SERI/TR-253-3196	
9. Performing Organization Name and Address Solar Energy Research Institute 1617 Cole Boulevard Golden, Colorado 80401		10. Project/Task/Work Unit No. ST712831	
		11. Contract (C) or Grant (G) No. (C) (G)	
12. Sponsoring Organization Name and Address		13. Type of Report & Period Covered Technical Report	
15. Supplementary Notes		14.	
16. Abstract (Limit: 200 words) This report documents the results of a study on the technical and economic potential of high-temperature central receiver systems for producing electricity. The study covered three advanced high-temperature (1000°-1400°C) central receiver concepts: the direct absorption receiver, the particle injection receiver, and the volumetric receiver. Each receiver was coupled with an intercooled steam-injected gas turbine engine mounted on the tower. Based on this analysis, the particle injection receiver has cost and performance advantages over the volumetric receiver and the direct absorption receiver for high temperatures. Although uncertainties associated with these systems discourage initiating a major program effort in the near term, several low-level activities were identified that if pursued will substantially reduce the degree of uncertainty and allow a more accurate estimation of the technical viability.			
17. Document Analysis a. Descriptors Central Receivers ; Direct-Contact Heat Exchangers ; Gas Turbine Engines ; Solar Concentrators ; Solar Thermal Conversion b. Identifiers/Open-Ended Terms c. UC Categories 235			
18. Availability Statement National Technical Information Service U.S. Department of Commerce 5285 Port Royal Road Springfield, Virginia 22161		19. No. of Pages 82	
		20. Price A05	